Check for updates

AGU ADVANCING EARTH AND SPACE SCIENCES

JAMES | Journal of Advances in Modeling Earth Systems®

RESEARCH ARTICLE
10.1029/2022MS003501

An Aerosol Optical Module With Observation-Constrained Black Carbon Properties for Global Climate Models

Ganzhen Chen[1,2], Jiandong Wang[1,2], Yuan Wang[3], Jiaping Wang[4], Yuzhi Jin[1,2], Yueyue Cheng[1,2], Yan Yin[1,2], Hong Liao[5], Aijun Ding[4], Shuxiao Wang[6], Jiming Hao[6], and Chao Liu[1,2]

[1]Collaborative Innovation Center on Forecast and Evaluation of Meteorological Disasters, Nanjing University of Information Science and Technology, Nanjing, China, [2]China Meteorological Administration Aerosol-Cloud-Precipitation Key Laboratory, School of Atmospheric Physics, Nanjing University of Information Science and Technology, Nanjing, China, [3]Department of Earth System Sciences, Stanford University, Stanford, CA, USA, [4]Joint International Research Laboratory of Atmospheric and Earth System Sciences, School of Atmospheric Sciences, Nanjing University, Nanjing, China, [5]Jiangsu Key Laboratory of Atmospheric Environment Monitoring and Pollution Control, Jiangsu Collaborative Innovation Center of Atmospheric Environment and Equipment Technology, School of Environmental Science and Engineering, Nanjing University of Information Science and Technology, Nanjing, China, [6]State Key Joint Laboratory of Environmental Simulation and Pollution Control, School of Environment, Tsinghua University, Beijing, China

Key Points:

- Observations of black carbon (BC) properties are implemented in the current aerosol optical module of Community Atmosphere Model version 6
- The modeled BC absorption enhancement and aerosol bulk optical properties are closer to the observations
- The BC top of the atmosphere direct radiative effect decreases from 0.37 to 0.28 W/m^2

Correspondence to:

J. Wang and C. Liu,
jiandong.wang@nuist.edu.cn;
chao_liu@nuist.edu.cn

Citation:

Chen, G., Wang, J., Wang, Y., Wang, J., Jin, Y., Cheng, Y., et al. (2023). An aerosol optical module with observation-constrained black carbon properties for global climate models. *Journal of Advances in Modeling Earth Systems*, *15*, e2022MS003501. https://doi.org/10.1029/2022MS003501

Received 4 NOV 2022
Accepted 16 SEP 2023

Author Contributions:

Conceptualization: Jiandong Wang, Chao Liu
Data curation: Ganzhen Chen, Jiandong Wang, Yuzhi Jin, Yueyue Cheng
Formal analysis: Jiandong Wang, Chao Liu
Funding acquisition: Jiandong Wang, Chao Liu
Investigation: Ganzhen Chen
Methodology: Ganzhen Chen, Chao Liu
Software: Ganzhen Chen
Writing – original draft: Jiandong Wang, Chao Liu

© 2023 The Authors. Journal of Advances in Modeling Earth Systems published by Wiley Periodicals LLC on behalf of American Geophysical Union. This is an open access article under the terms of the Creative Commons Attribution-NonCommercial-NoDerivs License, which permits use and distribution in any medium, provided the original work is properly cited, the use is non-commercial and no modifications or adaptations are made.

Abstract Atmospheric black carbon (BC) aerosols have been long-lasting uncertain components in environmental and climate studies. Global climate models (GCMs) potentially overestimate BC absorption efficiency due to a lack of consideration of complex BC microphysical and mixing properties. We extract multiple BC properties from observations and develop an aerosol optical module known as Advanced Black Carbon (ABC) in the framework of the Modal Aerosol Model version 4 (MAM4). The ABC module is implemented in the Community Atmosphere Model version 6 (CAM6) and evaluated by in situ and remote sensing observations. CAM6-ABC addresses the shortcomings of CAM6-MAM4 in terms of BC microphysical and mixing properties, particularly their size, mixing state and optical simulations. Sensitivity simulations show that the global BC absorption aerosol optical depth at 550 nm simulated by CAM6-ABC is reduced by ~29% compared with that in CAM6-MAM4. The BC absorption enhancement simulated by CAM6-ABC is reduced from ~2.6 of the default MAM4 to ~1.4, which is closer to the observed values (mostly less than 1.5). With improved BC absorption estimation, the biases of aerosol single-scattering coalbedo simulations are reduced by 18%–69% compared with global Aerosol Robotic Network observations. Moreover, the globally averaged BC direct radiative effect is reduced from 0.37 to 0.28 W/m^2 at the top of the atmosphere. Our new scheme alleviates the overestimation of BC absorption in GCMs by constraining BC microphysical and mixing properties when assessing aerosol radiative and climate effects, and it can be easily implemented in most modal-based aerosol modules of climate models.

Plain Language Summary As a climate warming agent in the atmosphere, black carbon (BC) aerosols remain largely uncertain in their light absorption. In global climate models (GCMs), the BC absorption efficiency tends to be overestimated due to insufficient consideration of the BC microphysical properties and mixing state. Our work quantifies the aerosol representation deficiency in GCMs due to the microphysical and optical properties and compensates for this deficiency in our improved BC and aerosol optical property representation. In this study, we analyze and summarize the key BC properties that highly influence their radiative effects based on multisource observations, for example, size distribution and mixing state, develop an improved aerosol optical module to better account for those observations, and implement this representation in a GCM. We use in situ observations to evaluate our module with improved BC and aerosol optical property representations. The results show that the overestimated BC absorption is much closer to the observations due to a more accurate representation of BC-related microphysical and mixing properties. Correspondingly, our improved BC representation weakens the modeled BC radiative and climate effects by as much as ~24%.

1. Introduction

Black carbon (BC) aerosol is the second-largest warming agent in the atmosphere, immediately after greenhouse gases (Jacobson, 2001; Masson-Delmotte et al., 2021; Pachauri et al., 2014; Y. Wang et al., 2013). Although the mass fraction of BC in atmospheric aerosols typically accounts for less than 10%, the contribution of BC

Writing – review & editing: Ganzhen Chen, Jiandong Wang, Yuan Wang, Jiaping Wang, Yuzhi Jin, Yueyue Cheng, Yan Yin, Hong Liao, Aijun Ding, Shuxiao Wang, Jiming Hao, Chao Liu

to aerosol absorption is generally larger than 50%, which plays a significant role in the Earth system radiative budget (Bond et al., 2013; Sand et al., 2021). From a climate change mitigation perspective, removing BC from the atmosphere is one of the most feasible approaches to curb global warming (Bond et al., 2013; Ramanathan et al., 2001). The Sixth Assessment Report (AR6) of the Intergovernmental Panel on Climate Change Report continues to report that the BC forcing has a wide range of uncertainty, that is, between −0.30 and 0.40 W/m^2 (Masson-Delmotte et al., 2021).

The radiative uncertainty arises mainly from the highly complex and mutable BC microphysical and optical properties during its aging processes (Y. Wang et al., 2018). Freshly emitted BC particles become mixed with other aerosols, which further enhances BC absorption due to the so-called "lensing effect" (China et al., 2013; Schnaiter et al., 2005). Absorption enhancement (E_{abs}) is defined as a key uncertain parameter in representing light absorption during the BC aging process (Masson-Delmotte et al., 2021; Matsui et al., 2018; Y. Wu et al., 2016). The E_{abs} of fresh BC, that is, unmixed BC, is 1, and as fresh BC ages, its E_{abs} increases. Large uncertainties exist in both observations and model simulations of E_{abs}. In-situ measurements show null or relatively weak E_{abs}, mostly within a range of 1 to less than 1.5 (see Table 1) (Cappa et al., 2012, 2019; S. Liu et al., 2015; D. Liu et al., 2017; C. Wu et al., 2018). However, from the perspective of model simulation, chemical transport models or Earth system models that assume an internally homogeneous mixed BC normally predict much larger E_{abs} values (Brown et al., 2021; Fierce et al., 2016; Peng et al., 2016). Consequently, the internally homogeneous mixing used in the optical treatments of most global climate models (GCMs) may significantly exaggerate BC warming effects.

The poorly modeled BC absorption efficiency and enhancement are largely attributed to the oversimplification of its microphysical properties and mixing states in current GCMs (Matsui et al., 2013; Riemer et al., 2019). GCMs mostly use modal or sectional (bin) methods for aerosol representation, which assume aerosols to be internally homogeneous mixtures within a certain mode/bin; thus, the BC components are uniformly distributed in all the aerosol particles of the mode/bin. Typical mode-based models include the Modal Aerosol Model version 4 (MAM4) in Community Atmosphere Model version 6 (CAM6), the aerosol-climate modeling earth system ECHAM5-HAM developed by European Centre for medium-range weather forecasts in Hamburg, the Multiconfiguration Aerosol TRacker of mIXing state in the Goddard Institute for Space Studies climate model, and the atmospheric component in the Geophysical Fluid Dynamics Laboratory coupled model (CM3) (Bauer et al., 2008, 2010; X. Liu et al., 2016, 2012; Stier et al., 2005; F. Zeng et al., 2011). The sectional/bin models include the Canadian Aerosol Module (CAM) in the third generation of the Canadian general circulation model and SALSA2.0 in the aerosol–chemistry–climate model ECHAM-HAMMOZ (Gong et al., 2002, 2003; Kokkola et al., 2018). In addition, the homogeneous or core-shell (CS) spherical particle assumption is commonly used in BC representation in GCMs without considering the complex BC morphology. The corresponding optical properties from internally homogeneous mixing or CS models ignore the influences of actual mixing and morphological properties, also resulting in an overestimated E_{abs} (Taylor et al., 2020). Alternatively, some GCMs simplify BC mixing states by using assumptions that are less physical or actual, for example, unique external mixing or fixed E_{abs} (Kokkola et al., 2018; Krol et al., 2005; X. Wang et al., 2014). To summarize, the treatments of the BC size distribution and mixing state in many GCMs are too simplified to accurately represent BC properties.

Moreover, with the significant uncertainties in BC influences on aerosol optical properties and radiative effects, some state-of-the-art aerosol models have been developed to better model BC-related procedures. For instance, Matsui (2017) introduced a 2-D sectional global aerosol model, that is, the aerosol two-dimensional bin module for formation and aging simulation version 2 (ATRAS2), which divides aerosols into 12 size bins and 8 BC mixing state bins (Matsui, 2017). Moreover, a Modal Aerosol Dynamics model for Europe including insoluble modes (MADE-in), consisting of seven modes characterized by particle size, composition and mixing state, was also developed (Aquila et al., 2011). In MADE-in, the BC aerosol is distributed in 4 modes, according to two sizes (Aitken mode and accumulation mode) and two BC mixing states (external and CS mixture). Furthermore, the size-resolved PartMC-MOSAIC model resolves the composition of individual particles with 19 species per particle. This particle-based model tracks the evolution of mixing states in aerosol processes and is applied only to box and single-column models due to the high computational cost (Curtis et al., 2017; Riemer et al., 2009; Zaveri et al., 2010).

In this study, we develop a new aerosol optical property model based on MAM4 with an advanced BC representation, namely, Advanced Black Carbon (ABC), and implement it into CAM6 of Community Earth System Model

19422466, 2023, 10, Downloaded from https://agupubs.onlinelibrary.wiley.com/doi/10.1029/2022MS003501 by Nanjing University Of, Wiley Online Library on [21/10/2023]. See the Terms and Conditions (https://onlinelibrary.wiley.com/terms-and-conditions) on Wiley Online Library for rules of use; OA articles are governed by the applicable Creative Commons License

Journal of Advances in Modeling Earth Systems

10.1029/2022MS003501

Table 1
Observed E_{abs} Data From Previous Studies

E_{abs} method	Longitude + Latitude	Location	Wave-length (nm)	Sampling duration	BC measurement	βabs measurement	E_{abs}	References
TD[a]	43.7°N 79.4°W	Toronto, Canada	760	2006.12–2007.1	OCEC	AE/PAS	1.6–1.9	Knox et al. (2009)
TD	37.5°N 122.2°W	California, USA	532	2010.5–2010.6	SP2	PAS	1.06 ± 0.006	Cappa et al. (2012)
TD	40°01′N 105°16′W	Boulder, USA	532	2010.9	SP2	PAS	1.3	Lack et al. (2012)
MAC[b]	22°38′N 114°5′E	Shenzhen, China	532	2011.8.25–2011.9.21	SP2	PAS	1.3	Lan et al. (2013)
TD	37.5°N 137.4°E	Noto Peninsula, Japan	532	2013.4.17–2013.5.14	SP2	PAS	1.06	Ueda et al. (2016)
MAC	53°28′N 2°18′W	Manchester, UK	532	2014.10.29–2014.11.10	SP2	PASS-3	1.0–1.3	D. Liu et al. (2017)
MAC	26.5°N, 80.3°E	Kanpur, India	781	2015.1.8–2015.2.28	SP2	PAX	1.8	Thamban et al. (2017)
MAC	23.8°N 113.2°E	Guangzhou, China	550	2012.2–2013.3	OCEC	AE	1.5 ± 0.48	C. Wu et al. (2018)
TD	34.1°N 117.5°W	Fontana, United States	532	2015.7.3–2015.7.15	SP2	PAX	1.07 ± 0.22	Cappa et al. (2019)
TD	36.8°N 119.8°W	Fresno, United States	532	2014.12.25–2015.1.12	SP2	PAX	1.22 ± 0.15	Cappa et al. (2019)
TD	32.0°N 118.7°E	Nanjing, China	532	2014.8.16–2014.8.28	SP-AMS	PASS-3	1.42 ± 0.40	Ma et al. (2020)
MAC	5.0°S 5.0°E	Southeast Atlantic Ocean	514	2017.8.16–2017.9.7	SP2	PAX	1.875 ± 0.375	Taylor et al. (2020)

[a]The TD method removes the coating material by heating the sample in a thermodenuder (TD) and then defines E_{abs} with $E_{abs} = b_{abs;\,ambient}/b_{abs;\,TD}$, where $b_{abs;\,TD}$ is corrected for particle losses. [b]The MAC method calculates E_{abs} using the MAC of coated and uncoated BC, which can be described by $E_{abs} = MAC_{ambient}/MAC_{bare}$, where MAC_{bare} is the mass absorption cross section of bare BC; its values are typically obtained from the literature.

19422466, 2023, 10, Downloaded from https://agupubs.onlinelibrary.wiley.com/doi/10.1029/2022MS003501 by Nanjing University Of, Wiley Online Library on [21/10/2023]. See the Terms and Conditions (https://onlinelibrary.wiley.com/terms-and-conditions) on Wiley Online Library for rules of use; OA articles are governed by the applicable Creative Commons License

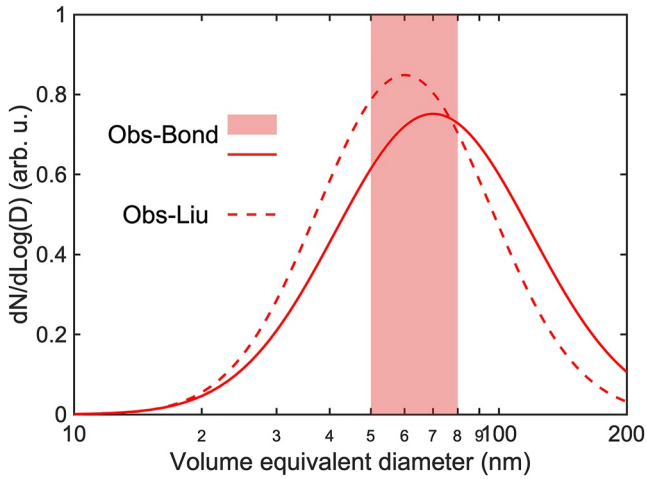

Figure 1. The normalized number size distribution of uncoated black carbon from in-situ observations of urban emissions (Bond et al., 2013) and mostly traffic sources (D. Liu et al., 2014). The red shading and red line represent observations from Tokyo and Nagoya (Japan) and Seoul (Korea) by Bond et al. (2013), while the red dashed line represents the observation from London by D. Liu et al. (2014).

version 2 (CESM2-CAM6) to improve the representation of BC microphysical and optical properties. Section 2 shows the in-situ observed data on BC microphysical (Section 2.1) and optical properties (Section 2.2). Section 3 describes the development of the observation-based ABC module regarding how BC aerosols are mixed with other components, and it is validated using observations. Section 4 evaluates the ABC module implemented in CAM6. Section 5 provides the conclusions for this work.

2. Methods and Data

2.1. Observed BC Microphysical and Mixing Properties

Many field campaigns and laboratory measurements have been analyzed to determine BC microphysical characteristics and mixing states that significantly influence its optical properties. We consider some essential facts about BC properties derived from global observations in our model development: (a) BC cores show a lognormal distribution with count median diameters (CMDs) ranging from 50 to 80 nm for urban emissions; (b) different-sized BC cores have similar coating thicknesses (CTs). Further details are provided in the following paragraphs.

In the present study, the size and number fraction of the BC core and BC-containing particles are observed by a single particle soot photometer (SP2). As one of the most reliable particle-resolved instruments, SP2 obtains various particle sizes and BC mixing states in the atmosphere by detecting scattered laser signals from soot samples for individual sizes of BC and BC-containing particles (Gao et al., 2007). Ambient soot is extracted from ambient air through a heated inlet. Then, the ambient soot passes through a laser beam and is evaporated into BC through heating. In the process of soot particle evaporation, the decrease in the scattering intensity reflects the CT of the BC-containing particles. Through this method, the sizes of particle-resolved BC and BC-containing particles are derived from scattered signals.

The BC size distribution was measured in different locations and from different sources. In urban areas of Tokyo, Nagoya (Japan) and Seoul (Korea), Bond et al. (2013) reported that BC particles from fossil fuel (FF) combustion show lognormal distributions with CMDs ranging from 50 to 80 nm (red shade in Figure 1). According to the winter observation in London by D. Liu et al. (2014), the CMDs of uncoated BC particles emitted by traffic-dominated sources are approximately 60 nm. Thus, the BC size distribution applied in our newly developed module is adopted from Bond et al. (2013), that is, 70 nm.

In addition to the BC size distributions, the distributions of the CTs of different-sized BC particles are also important for their optical properties. We regard the BC size (D_{BC}) and particle size (D_p) as the volume equivalent spherical diameters of the BC component and overall BC-containing particles, respectively. Briefly, SP2 uses laser-induced incandescence and light scattering signals to determine D_{BC} and D_p. Artifacts from SP2 exist due to charring of the organic coating material in the heating of refractory BC, which depends on the laser power (Sedlacek et al., 2018; Zhang et al., 2023). However, in our study, the laser power varied over a range of 3.4–3.5 V, which is above the threshold to detect refractory BC with high efficiency (Kompalli et al., 2020). Although we cannot exclude the additional contribution of refractory BC from charring organic coating material, its bias likely occurs outside our laser voltage range. In summary, we acknowledge that there is an overestimation of refractory BC from charring in the detection, which is difficult to quantify and not large enough to affect our conclusions.

Thus, the mixing state of each detected BC-containing particle is quantified by CT, defined as $CT = (D_p - D_{BC})/2$. Here, we use ambient soot data sampled in Nanjing, China (February to June 2020), Tokyo, Japan (August 2012) (Moteki et al., 2014), and Sacramento, USA (15 June 2010) (Zaveri et al., 2012). To further understand BC mixing processes, we investigate the relationship between BC size and aged BC-containing particle size in different stages of the aging process to obtain our conclusions. Figure 2 shows the CT distributions (blue violin plots) in the three locations at different D_{BC} values. The CTs at the three locations all show similar geometric means, which vary with different D_{BC} values (yellow dots), specifically, 36.4 nm in Nanjing (Figure 2a), 11.0 nm in Tokyo (Figure 2b), and 22.0 nm in Sacramento (Figure 2c), as demonstrated in our previous study (J. Wang et al., 2023).

19422466, 2023, 10, Downloaded from https://agupubs.onlinelibrary.wiley.com/doi/10.1029/2022MS003501 by Nanjing University Of, Wiley Online Library on [21/10/2023]. See the Terms and Conditions (https://onlinelibrary.wiley.com/terms-and-conditions) on Wiley Online Library for rules of use; OA articles are governed by the applicable Creative Commons License

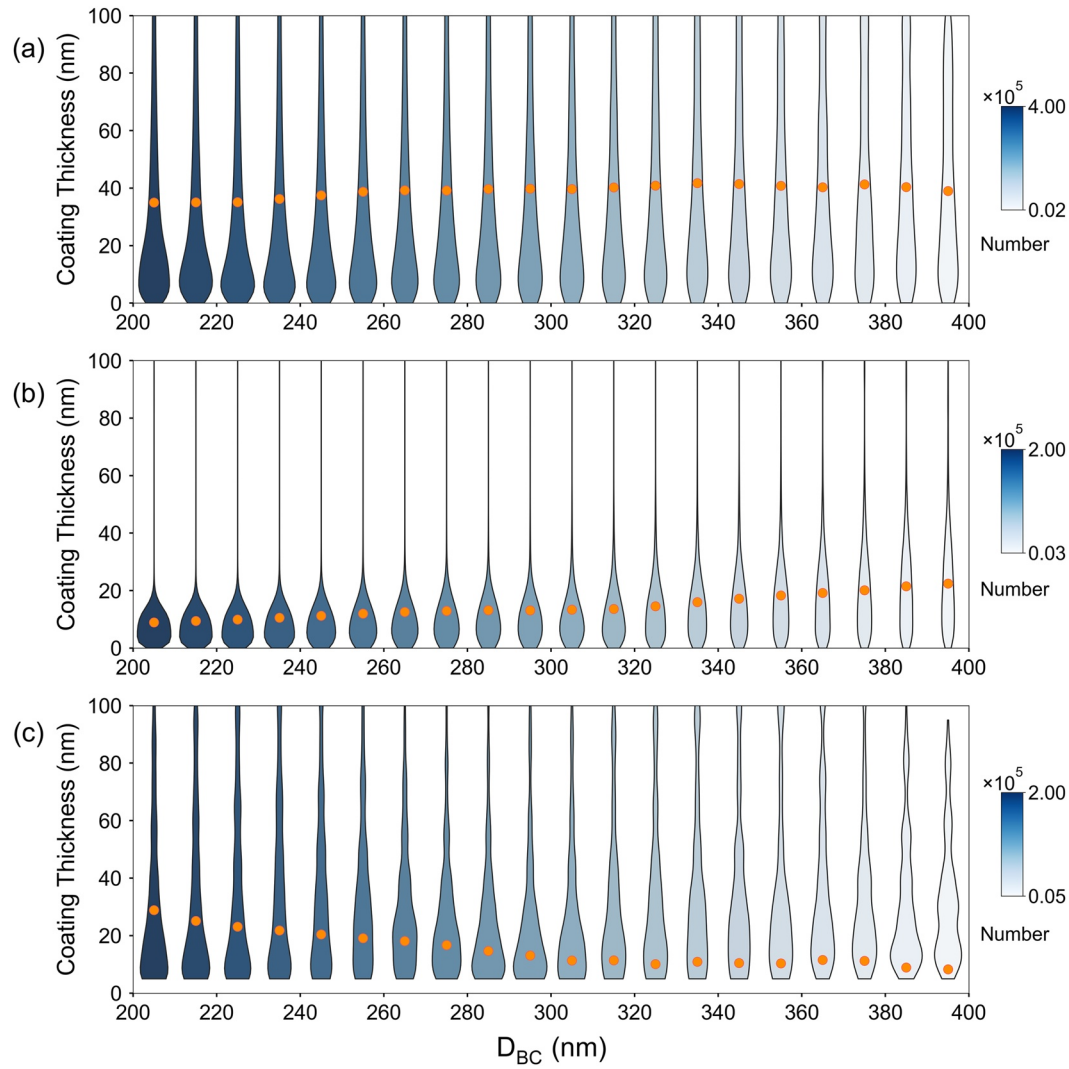

Figure 2. Violin plots showing the distribution of coating thickness (CT), that is, $(D_p - D_{BC})/2$, in each D_{BC} bin for Nanjing, China (a), Tokyo, Japan (b) and Sacramento, USA (c). The color scales show the number of each bin. The orange dots show the geometric means of the CT in each D_{BC} bin. The particles are divided into several bins with a 10 nm interval.

Different shades of blue represent the number of particles, where a lighter blue indicates fewer particles. Due to the deficiency in the SP2 detection efficiency, we analyze BC size bins only ranging from 200 to 400 nm, excluding particles with diameters of less than 200 nm (T. Li et al., 2012). Note that CTs for BC-containing particles with different D_{BC} values are basically similar and are changeable globally under different circumstances. Thus, an equal-CT feature for different D_{BC} is possible to simplify the BC mixing representation in GCMs.

2.2. Observed Aerosol Optical Properties

The light absorption enhancement, E_{abs}, of BC particles is one of the most important but uncertain parameters in quantifying BC radiative effects and is defined as the ratio between the mass absorption coefficients (MACs) after and before mixing with other components. The E_{abs} greatly varies due to BC particle properties as well as measurement uncertainties. Global E_{abs} measurements are summarized in Table 1. The E_{abs} values range from 1 to 1.8 when using technologically advanced instruments for BC microphysical and optical properties, such as the SP2, soot particle aerosol mass spectrometer (SP-AMS), organic carbon and elemental carbon (OC-EC) analyzer, photoacoustic spectrometer (PAS), photoacoustic extinction meter (PAX), three-wavelength photoacoustic soot spectrometer (PASS-3) and aethalometer (AE). Two approaches are used to retrieve the absorption of bare and

19422466, 2023, 10, Downloaded from https://agupubs.onlinelibrary.wiley.com/doi/10.1029/2022MS003501 by Nanjing University Of, Wiley Online Library on [21/10/2023]. See the Terms and Conditions (https://onlinelibrary.wiley.com/terms-and-conditions) on Wiley Online Library for rules of use; OA articles are governed by the applicable Creative Commons License

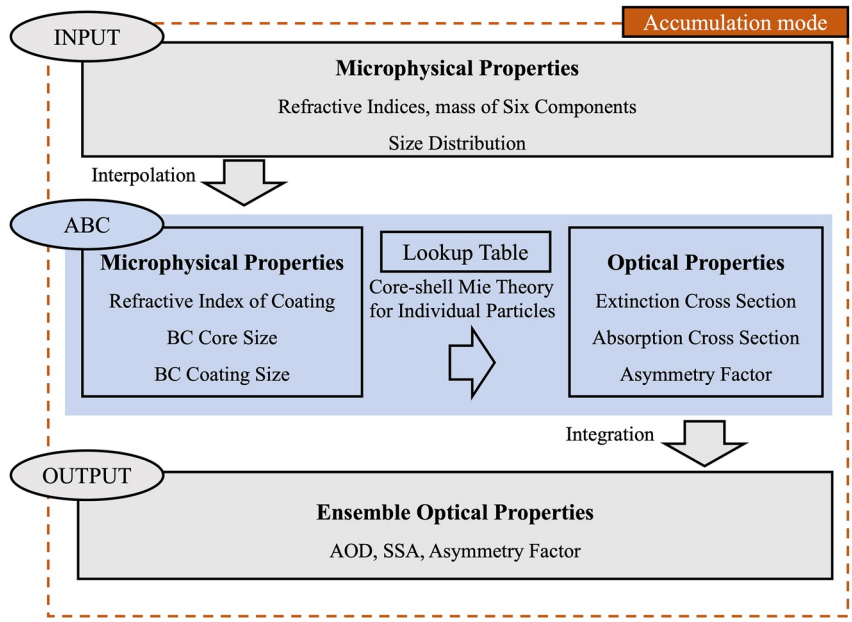

Figure 3. Diagram of the Advanced Black Carbon module structure in the accumulation mode of Community Atmosphere Model version 6.

aged BC and determine the value of E_{abs}, namely, the thermodenuder (TD) method and the MAC extrapolation method. The TD method may lead to biased low E_{abs} due to low-volatility brown carbon coating (Cappa et al., 2013; Shetty et al., 2021); however such underestimation would not change the conclusions shown in the table, which are well supported by other observations (Lan et al., 2013; D. Liu et al., 2017; C. Wu et al., 2018). Table 1 indicates that E_{abs} tends to be less than 1.5. Note that the E_{abs} observations shown are from shortwaves at average states of the aging process.

Moreover, we use in situ observations from the Aerosol Robotic Network (AERONET), which is a global ground-based aerosol network based on spectral observations of CIMEL CE318 (Dubovik & King, 2000; Holben et al., 1998). The AERONET project provides spectral aerosol optical depth (AOD), inversion products, and precipitable water data for diverse aerosol regimes (http://aeronet.gsfc.nasa.gov/). The inversion products include globally distributed observations of single-scattering albedo (SSA), which has three data quality levels: Level 1.0 (unscreened), Level 1.5 (cloud-screened and quality controlled), and Level 2.0 (quality-assured). In our study, level 2.0 monthly data from AERONET sites worldwide from 2011 to 2016 are used for evaluation.

The existing in situ measured and retrieved BC microphysical properties, E_{abs} and overall aerosol optical properties provide the most valuable indications for model development and improvement. This study aims to introduce an improved aerosol optical property model by better presenting BC and its mixing states in the optical simulations of GCMs and using the aforementioned observations for both model evaluation and development. Note that the equal-CT characteristic of the SP2 observations (Figure 2) is further validated in Section 3.

3. Development of the ABC Module and Model Description

3.1. Aerosol Optical Module With Advanced BC (ABC) Treatment

In this study, we establish a new aerosol module, that is, ABC, for a new BC representation that is applied in the accumulation mode of CAM6. The ABC simulates the same aerosol number and mass as the MAM4 of the default CAM6 but treats the BC mixing state differently in the optical calculation. In contrast to CAM6-MAM4, we distinguish BC-containing and non-BC particles from all particles in the accumulation mode in ABC. As the diagram shows (Figure 3), our new aerosol optical module, ABC, utilizes the CS Mie theory to construct a lookup table for the optical properties of aged BC in the accumulation mode, in which most internally mixed BC particles coexist with soil dust, secondary organic matter (OM), primary OM, sulfate and sea salt. In the 4-D Mie lookup table, the real and imaginary parts of the coating mixture, BC core sizes and coating sizes are used in the CS

19422466, 2023, 10, Downloaded from https://agupubs.onlinelibrary.wiley.com/doi/10.1029/2022MS003501 by Nanjing University Of, Wiley Online Library on [21/10/2023]. See the Terms and Conditions (https://onlinelibrary.wiley.com/terms-and-conditions) on Wiley Online Library for rules of use; OA articles are governed by the applicable Creative Commons License

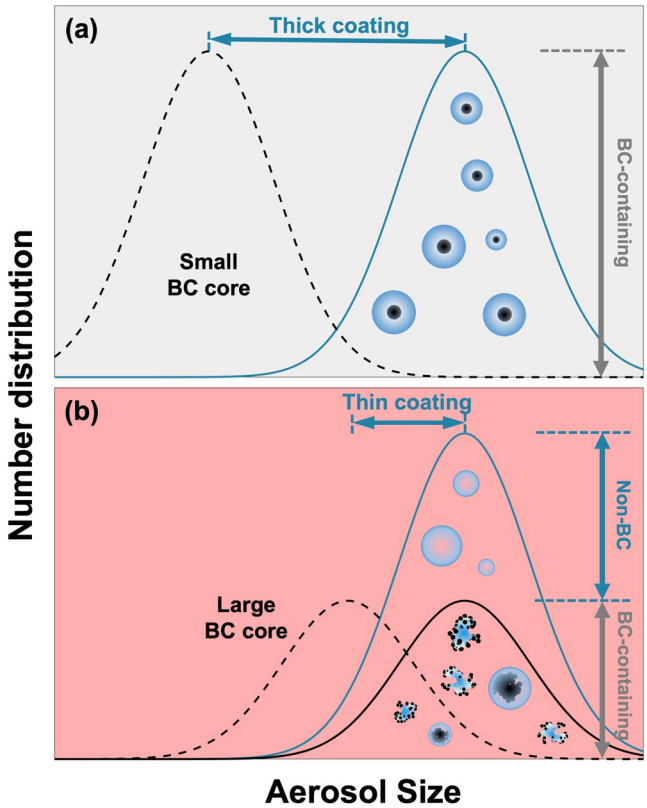

Figure 4. Conceptual schematics of the core-shell (CS) treatment and Advanced Black Carbon (ABC) for black carbon (BC) in Community Atmosphere Model version 6. (a) The CS treatments result in a small BC size, thick coating and 100% proportion of BC-containing particles, leading to artificial absorption enhancement. (b) ABC adopts the observed BC size distribution and mixing states, where only a certain fraction of accumulated particles encapsulate the BC component.

Mie model to compute the corresponding absorptive cross section, extinction cross section and asymmetry factor of individual particles. For the optical calculation procedure in CAM6, first, the aerosol microphysical properties, including the refractive indices of the coating, volume fractions of different species, median radius and number concentration in the mode, are input into ABC. After linear interpolation by the 4-D Mie lookup table and integration of individual particles into 30 size bins, the AOD, SSA and asymmetry factor of the ensemble aerosols are exported as the optical simulation results.

3.2. BC Microphysical Model in the ABC Module

There is a distinct improvement from the simple CS model to the ABC module in CAM6 with respect to the size distribution for BC-containing and non-BC particles. Compared with the conventional CS model, ABC optimizes BC treatment with a more reasonable aging process and mixing state, as shown in the conceptual schematics in Figure 4. In the accumulation mode, the new model first enlarges the BC size and limits the BC-containing particle number fraction, which results in a thinner coating. The small BC size, thick coating and 100% proportion of BC-containing particles in the conventional model are not consistent with the observations (Figure 4a) (L. Chen et al., 2020; Sun et al., 2022). First, our new scheme introduces a more realistic and larger BC core size distribution, which results in a lower BC particle number than the total aerosol number in the mode. The number differences are the numbers of non-BC particles. Second, by adopting the CMD of the mode for BC-containing particles, the coating amount/thickness of single particles is reduced. Because we fix only the BC core size distribution, the CTs still differ among cases, representing the spatiotemporal variations in BC mixing states. The size-resolved mixing structures can be independently and efficiently simulated in the optical property simulations, and the computational burden is similar to that of the default model. These treatments apply to all aerosols in the accumulation mode and are independent of BC sources, and the BC aging process between the primary carbon mode and accumulation mode in CAM6 is unaffected.

The mixed BC morphology is also considered in the development of the ABC module. In contrast to the idealized homogeneous or CS spheres that are assumed in most aerosol optical property estimations, ambient BC particles and mixed particles show highly complex and irregular geometries. In the real atmosphere, BC particles from transmission electron microscopy (TEM) images are mostly chain-like or compact aggregates with many monomers (J. Li et al., 2003), and the morphology of mixed BC could be more complicated and irregular (China et al., 2013). The complexity of BC morphology also accounts for uncertainties in radiative effects (Chakrabarty et al., 2014). In fact, such irregular features can be well represented numerically (Chakrabarty et al., 2007; C. Liu et al., 2012; Yurkin & Hoekstra, 2011) but are rarely considered due to the computational burden and lack of detailed parameterizations in GCMs. In this study, we consider morphological influences by numerically constructing irregular BC-containing particles and accurately simulating their optical properties. BC cores in the coated BC model are extensively treated as fractal aggregates (Köylü et al., 1995), and both spherical coating geometries and their position relative to the BC aggregates are considered (Adachi et al., 2010; Y. Wang et al., 2017). Figure 5 compares some examples of TEM images and our numerically generated BC-containing particles. According to the various relative positions of the BC aggregates to the coating and compactness of the BC aggregates, two kinds of microphysical models for mixed BC are constructed to represent the complex BC morphology. From the upper to lower row, BC aggregates that are partly coated and totally coated by spherical material are shown in Figure 5. To account for the complexity of BC particles in the atmosphere, particle parameters, including uncoated BC morphologies, sizes and refractive indices, are randomly generated using diffusion-limited cluster aggregation following C. Liu et al. (2019). Then, an accurate and efficient optical property algorithm, that is, the discrete dipole approximation (DDA), is used to model the light scattering properties of particles with

19422466, 2023, 10, Downloaded from https://agupubs.onlinelibrary.wiley.com/doi/10.1029/2022MS003501 by Nanjing University Of, Wiley Online Library on [21/10/2023]. See the Terms and Conditions (https://onlinelibrary.wiley.com/terms-and-conditions) on Wiley Online Library for rules of use; OA articles are governed by the applicable Creative Commons License

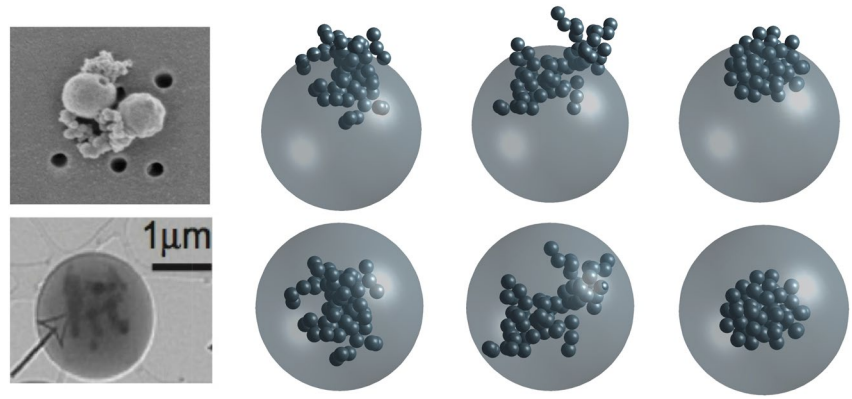

Figure 5. Examples of black carbon morphologies from transmission electron microscopy images (J. Li et al., 2003) and numerically generated irregular particles.

different sizes and random shapes (Yurkin et al., 2007; Yurkin & Hoekstra, 2011). Variations of more than 50,000 randomly irregular particles are generated to evaluate their influences on the optical simulations. Specifically, the volume equivalent D_{BC} of 70 nm, the volume equivalent D_p from 72 to 130 nm, and the BC refractive index (m_{core}) of 1.95 + 0.79i are all consistent with those of the irregular aggregate model for a visible wavelength (550 nm). These BC microphysical variables, such as the fractal dimension (D_f, from 2.2 to 2.8), the real part of the refractive index of the coating ($Re_{coating}$, from 1.3 to 1.5), the fractal prefactor ($k_0 = 1.2$) and the number of monomers in the aggregate N_s ($1 \sim 125$), are accounted for in the sensitivity simulations of the irregular BC model.

3.3. Optical Properties in the ABC Module

The aforementioned BC microphysical properties are possible factors influencing its optical properties, but they have not been explicitly considered in the current GCMs. We quantify their impacts and improve their treatments in CAM6 using the optical simulation module. First, different-sized BC particles are coated with different CTs. We use SP2 observations to validate the similar CT features of the BC optical properties, as mentioned in Section 2.1. For a certain sized D_{BC}, we average the optical properties of BC single particles with polydisperse CTs (according to the CT distributions in Figure 2) and compare them with those based on a monodisperse CT; this comparison is shown in Figure 6. The SP2 CT distributions from Figure 2 are used here, and the particles are treated as concentric spheres with a BC core and a coating shell of scattering particles. For the monodisperse counterpart, an equivalent volume CT value is derived for optical calculation. Specifically, the BC and BC-containing particles are divided into 40 size bins ranging from 200 to 600 nm. In every BC size bin, we calculate the effective absorption and scattering with all BC-containing bins (polydisperse) or with one equivalent-volume BC-containing particle size (monodisperse).

Figures 6a–6f compares BC absorption cross sections (C_{abs}) and scattering cross sections (C_{sca}) by a polydisperse and monodisperse method in the three cities mentioned above. The differences between the absorption cross sections of the polydisperse and monodisperse results based on SP2 measurements in these cities are mostly within 5%. Figures 6g and 6h shows that the BC MAC and mass scattering coefficient (MSC) vary with CT. We assume a BC m_{core} of 1.95 + 0.79i and a coating refractive index ($m_{coating}$) of 1.4 + 0.0i. Here, the lognormal distribution with a volume median diameter of 70 nm and a geometric standard deviation (σ_g) of 1.8 is considered for the BC core part. As illustrated in Figure 6g, BC MAC increases sharply and linearly as CT increases from 0 to less than 100 nm and increases less sharply when CT is between 100 and 200 nm. This result implies that BC absorption cannot increase indefinitely with increasing CT. Thus, we can replace the highly complex CT distributions with a single equivalent CT value for BC absorption simulations. Moreover, the similar CTs at different D_{BC} values indicated in Figure 2 could further simplify the BC mixing representation as a particle-to-particle shift from the D_{BC} distribution to the D_p distribution (as illustrated in Figure 4b). Namely, for sites in diverse environments, the CT distribution shows self-similarity; that is, BC with different core sizes has a similar CT in every particle population (J. Wang et al., 2023). Although Fierce et al. (2016) showed E_{abs} discrepancy due to particle-to-particle heterogeneity in CT, we found a unified and universally applicable distribution pattern that was not apparent in Fierce et al. (2016). The main differences between our study and that of Fierce et al. (2016)

19422466, 2023, 10, Downloaded from https://agupubs.onlinelibrary.wiley.com/doi/10.1029/2022MS003501 by Nanjing University Of, Wiley Online Library on [21/10/2023]. See the Terms and Conditions (https://onlinelibrary.wiley.com/terms-and-conditions) on Wiley Online Library for rules of use; OA articles are governed by the applicable Creative Commons License

19422466, 2023, 10, Downloaded from https://agupubs.onlinelibrary.wiley.com/doi/10.1029/2022MS003501 by Nanjing University Of, Wiley Online Library on [21/10/2023]. See the Terms and Conditions (https://onlinelibrary.wiley.com/terms-and-conditions) on Wiley Online Library for rules of use; OA articles are governed by the applicable Creative Commons License

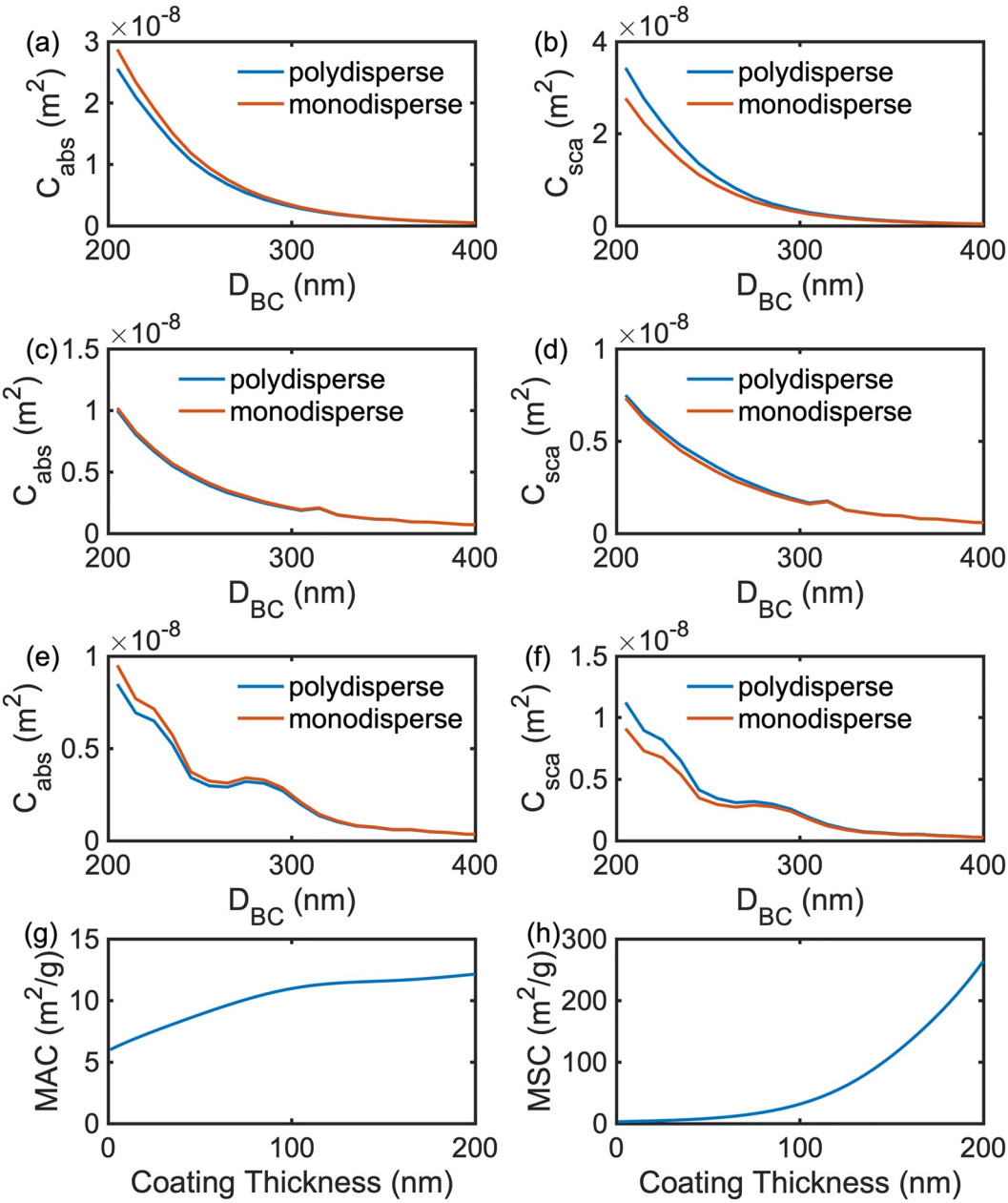

Figure 6. Comparison of absorption cross section (C_{abs}) and scattering cross section (C_{sca}) as a function of measured D_{BC} between polydisperse coating thicknesses (CTs) and a monodisperse CT in each D_{BC} bin based on soot photometer measurements. (a, b) Nanjing, China (c, d) Tokyo, Japan and (e, f) Sacramento, USA. (g, h) Mass absorption coefficient (MAC) and mass scattering coefficient (MSC) of black carbon (BC) for different CTs at a wavelength of 550 nm.

are due to the use of different coordinate systems. Therefore, the two studies are not necessarily in conflict but rather reflect the complexity of the BC mixing state. In this way, the complex relationship between D_{BC} and D_P in SP2 is simplified as a one-to-one relationship while their optical properties, especially the absorption, remain consistent. Once two of the three variables, that is, the D_{BC} size distribution, D_p size distribution and CT, are known, the numbers of BC-containing particles can be set for the optical simulations. Here, we can obtain the D_{BC} and D_p size distributions from observations and CAM6, respectively. Then, the CT is obtained following $(D_p - D_{BC})/2$.

Subsequently, we try to efficiently consider the influence of complex particle morphologies on the optical properties by adjusting the CS results with predefined scaling factors. To obtain these adjustment factors, the optical

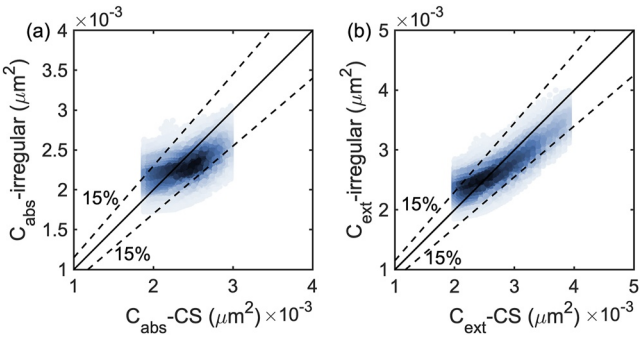

Figure 7. Comparison between C_{abs} (a) and C_{ext} (extinction cross section) (b) based on the core-shell (CS) model and irregular black carbon model. The darker area represents a higher density of points with over 50,000 randomly generated particles. The dashed lines represent a relative difference of 15% between the irregular and CS models.

properties of BC-containing particles with complex morphologies and CS spheres are compared. As illustrated in Figure 5, irregular particles that are similar to actual particles can be numerically constructed, and their optical properties can be accurately calculated using the DDA algorithm (Yurkin & Hoekstra, 2011) and compared with those of the corresponding CS spheres (by the CS Mie algorithm). Figure 7 illustrates a particle-to-particle comparison of the absorption and scattering cross sections for the irregular (BC as aggregate structures) and CS spherical particles. The microphysical properties in the irregular aggregate model and CS model are described in Section 3.2. The C_{abs} of fractal-like-based particles could be either 30% larger or smaller than the CS counterparts, while the average of C_{abs} with the irregular BC model (2.31×10^{-3} μm^2) is ∼3% lower than that of the CS model (2.39×10^{-3} μm^2). The results in our study are inconsistent with those of Chakrabarty and Heinson (2018). Specifically, Chakrabarty and Heinson (2018) utilized the skin depth, which is related to the incident wavelength and the imaginary part of the BC refractive index, to represent the absorbing capacity. As the BC core size in the CS model increases to the skin depth, the MAC_{BC} reaches an upper limit. However, the monomer in aggregate counterparts is small enough as the total absorbing contribution, accounting for an increasing MAC_{BC} from the CS model to the coated aggregate model with bare BC from 107 to 314 nm. However, in our study, the results of decreasing MAC from the CS to the irregularly coated aggregate model are consistent with Fierce et al. (2016), Romshoo et al. (2022), and Y. Wang et al. (2021), while this decrease could be different due to different choices of BC and coating equivalent sizes. Compared with previous studies, such as Luo et al. (2019), our study simulates a smaller BC size and thin coating (equivalent CT <60 nm). The mean value of C_{ext} with the irregular BC model (2.75×10^{-3} μm^2) is ∼3% lower than that of the CS model (2.82×10^{-3} μm^2). Such morphological variations would introduce mean relative differences of ∼3% for both absorption (Figure 7a) and extinction (Figure 7b). By linear regression, we obtain scaling factors of 0.97 and 1.03 for absorption and extinction, respectively, using the CS model.

Another factor that influences the absorption of mixed BC particles is the relative position between the BC core and coating component (C. Liu et al., 2017; C. Zeng et al., 2019). In the CS model, the BC core is in the center of the coating, that is, a concentric spherical structure. However, the BC core can be located anywhere within the coating sphere. Figure 8 shows the absorption cross sections of coated BC particles as functions of the distance of the BC core from the coating center. A thicker CT means a greater BC size ratio of coating to core (D_p/D_{BC}), within 1 ∼ 20 (blue histograms in Figure 8c), in CAM6-MAM4 relative to 1∼5 (red histograms in Figure 8c) in CAM6-ABC, accounting for the smaller BC core size (∼10 nm) in CAM6-MAM4 and the larger BC core size (70 nm) in the CAM6-ABC model. The E_{abs} reaches a maximum when the BC core is located at the center and gradually decreases as it moves toward the edge of the coating (Figure 8a). However, such optical effects of the BC core relative position are significant only for particles with a relatively large CT. When the D_p/D_{BC} is less than 5, the impact of different relative positions of the BC core on E_{abs} can nearly be ignored (Figure 8b). Notably, in this study, the D_p/D_{BC} variations have a limited effect on BC E_{abs}, so such a CS distance effect is ignored.

Finally, to explore the optical effect caused by different BC mixing states and size distributions, an offline aerosol optical calculation is performed. In the offline simulation, we set m_{core} to 1.95 + 0.79i and $m_{coating}$ to 1.5 + 0.005i, which are all consistent with the settings of the online CAM6 simulation. We calculate BC MAC in every CMD for 30 different radii between 0.01 and 10 μm, with a lognormal size distribution at a geometric standard deviation (σ_g) of 1.8, applying the CS Mie model. Figure 9 shows the impact of BC size and CT distributions on BC MAC in the default CAM6-MAM4 and CAM6-ABC models. Under the condition of a thin CT (less than 30 nm), the BC MACs increase at first and then decrease with increasing CMD. As the CT becomes thicker, up to 30 nm, the BC MACs directly decrease with increasing CMD. In the default CAM6 model, where the BC CMD ranges from 10 to 40 nm and the CT ranges from 40 to 60 nm, the MAC of BC-containing particles ranges from 10 to 16 m^2/g (i.e., shaded blue area indicated in Figure 9). In contrast, in the CAM6-ABC model, where the BC CMD ranges from 60 to 80 nm and the CT ranges from 10 to 30 nm, the MAC of BC-containing particles ranges from 6 to 8 m^2/g (i.e., shaded red area in Figure 9). Therefore, the different BC sizes in different-sized BC-containing particles largely determine BC MAC, accounting for higher BC MAC values in the CAM6-MAM4 model and lower values in the CAM6-ABC model.

19422466, 2023, 10, Downloaded from https://agupubs.onlinelibrary.wiley.com/doi/10.1029/2022MS003501 by Nanjing University Of, Wiley Online Library on [21/10/2023]. See the Terms and Conditions (https://onlinelibrary.wiley.com/terms-and-conditions) on Wiley Online Library for rules of use; OA articles are governed by the applicable Creative Commons License

19422466, 2023, 10, Downloaded from https://agupubs.onlinelibrary.wiley.com/doi/10.1029/2022MS003501 by Nanjing University Of, Wiley Online Library on [21/10/2023]. See the Terms and Conditions (https://onlinelibrary.wiley.com/terms-and-conditions) on Wiley Online Library for rules of use; OA articles are governed by the applicable Creative Commons License

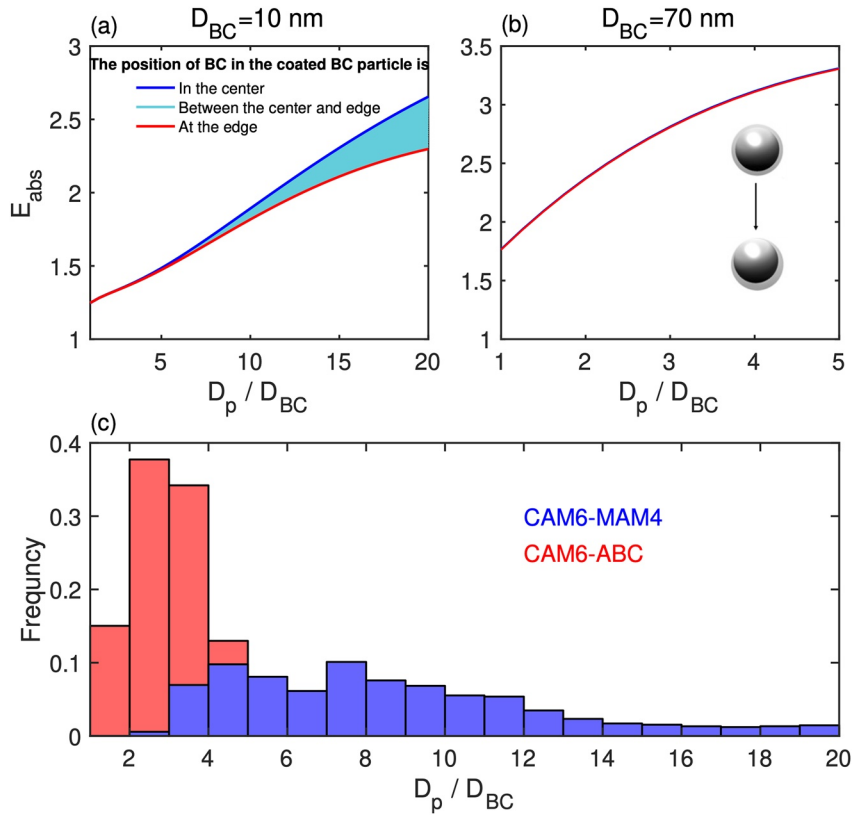

Figure 8. (a, b) Influence of black carbon (BC) core positions (from the central to inscribed sphere) on BC absorption enhancement (E_{abs}) in the core-shell model as a function of the size ratio of the shell to the core (D_p/D_{BC}). (c) D_p/D_{BC} distribution in the Community Atmosphere Model version 6 (CAM6)-Modal Aerosol Model version 4 (MAM4) and CAM6-Advanced Black Carbon (ABC) models.

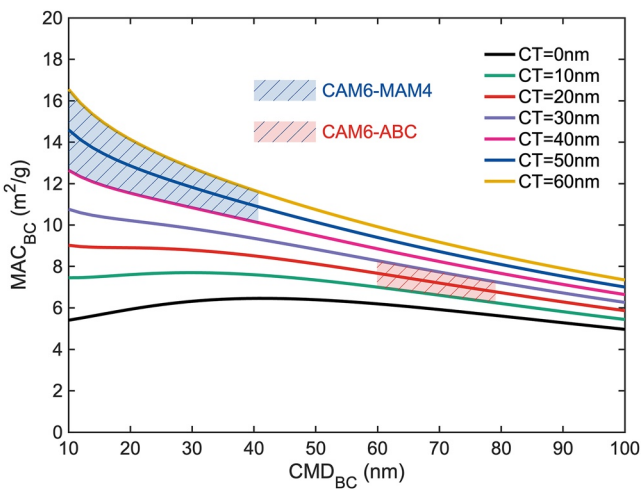

Figure 9. Comparisons of black carbon (BC) mass absorption coefficient (MAC) between the default Community Atmosphere Model version 6 (CAM6)-Modal Aerosol Model version 4 (MAM4) and CAM6-Advanced Black Carbon (ABC) models in different BC size distributions (coating thickness [CT]). BC MAC varies as a function of the count median diameter (CMD) of the BC size distribution and the CT in BC-containing particles. The shaded areas represent the CMD and the corresponding CT ranges in the default CAM6-MAM4 and CAM6-ABC models.

Section 3.2 focuses on BC microphysical properties related to the particle mixing process, while Section 3.3 focuses on the conclusions related to BC optical calculations. For BC optical properties, Section 3.3 shows our conclusions, including that the equal-CT characteristic (a CS model with the same CT value for different bare BC sizes) has been evaluated through three in-situ observations; 3% scaling factors can be applied for C_{abs} and C_{ext} to represent BC irregularity; and the position of the BC core can be ignored. Simultaneously, based on these conclusions, we calculate the BC MAC varying with different BC size distributions and different CTs in the CS model. The optical difference between the CAM-ABC and CAM-MAM4 models is displayed.

3.4. CAM6 Setup and Experimental Design

We use the CESM2-CAM6 with the aerosol optical properties provided by MAM4 (Danabasoglu et al., 2020) and simulate a case for the present-day climatology (2010) with the CMIP6-based emissions for aerosol and precursor gases. The optical module of CAM6 adopts a parameterization scheme for internally mixed aerosols, where the wet refractive index and wet surface radius are used to calculate the aerosol specific absorption, specific extinction and asymmetry factor (Ghan & Zaveri, 2007). The shortwave radiative transfer calculation is provided by the Rapid Radiative Transfer Model for General circulation models (Mlawer et al., 1997). In the radiative module, the AOD, SSA and asymmetry factor are the parameters that determine the

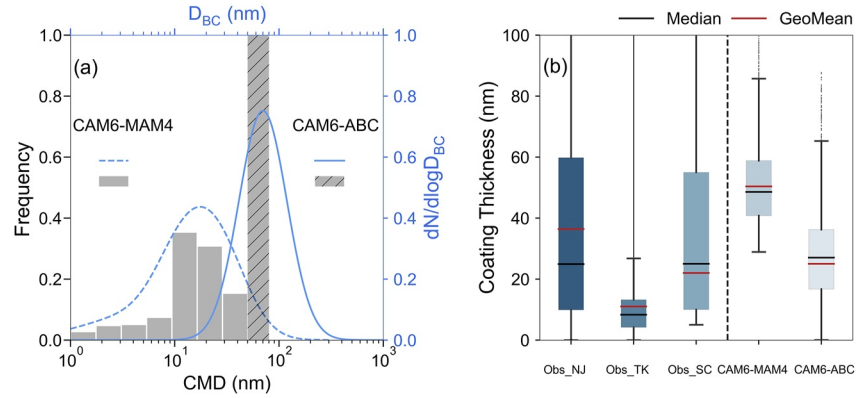

Figure 10. Observed and modeled black carbon (BC) microphysical and mixing properties. (a) Typical observed and default Community Atmosphere Model version 6 (CAM6)-modeled BC size properties. Occurrence frequencies of BC count median diameter (CMD) of the default CAM6-Modal Aerosol Model version 4 (MAM4) (gray histogram) and CAM6-Advanced Black Carbon (ABC) (gray histogram with slashes). An averaged BC size distribution in the default CAM6-MAM4 (blue dashed curve) and CAM6-ABC derived from observations of Bond et al. (2013) (blue solid curve), which is used in our new model. (b) Coating thickness distributions from soot photometer observations (Nanjing [NJ], China; Tokyo [TK], Japan; and Sacramento [SC], USA) (Moteki et al., 2014), the default CAM6-MAM4 and the CAM6-ABC scheme. In panel (b), the boxes are created from the 25th to 75th percentile as lower and upper sides. The black and red lines within the boxes represent the median value and geometric mean value. The lower (upper) boundaries (the whiskers) are the minimum (maximum) values excluding any outliers.

aerosol radiative properties. The solar spectrum is divided into 14 wave intervals from 0.2 to 12.2 μm. The delta-Eddington approximation is used to compute the reflections and transmissions in the atmosphere, assuming homogeneously mixed layers. The BC-induced radiative effects are estimated by the differences in the scenarios with and without BC by using the diagnostic calculations of CAM6. Global horizontal resolutions of 1.9° latitude × 2.5° longitude and 32 vertical layers (~40 km) are used. Our simulation is performed for 4 years, in which the first year is used for spin-up and the remaining years are used for optical and radiative analysis. To match the AERONET data with CAM6, the simulation period is set to 6 years between 2011 and 2016.

In the default CAM6, various kinds of aerosols are divided into 4 modes (primary carbon mode, Aitken mode, accumulation mode and coarse mode), with external mixing between modes and internal mixing within modes. As the control run case, the default optical parameterization (CAM6-MAM4) is applicable to homogeneously mixed aerosols but overlooks the CS mixture that is more suitable for the BC mixing state. We adopt a CS Mie model to develop a new optical parameterization (CAM-ABC). The CAM6-ABC simulation partitions the coating mass to fewer particles, resulting in a polydisperse distribution with a CS model of BC-containing and non-BC particles. Therefore, in the process of developing a new optical parameterization, CAM6-MAM4 and CAM6-ABC are used as the model experiments for aerosol optical evaluation.

4. ABC Performance

4.1. BC Microphysical Properties

The CAM6-ABC module is better at simulating a more reasonable BC size and CT than CAM6-MAM4 in the BC mixing process compared with in situ observations (see Figure 10). Figure 10 compares the observed and modeled (from the MAM4 and ABC modules) BC microphysical and mixing properties that mostly influence aerosol light absorption. In the default CAM6-MAM4, due to internally homogeneous mixing, the BC mass is uniformly distributed in each particle in the accumulation mode, accounting for equivalent BC CMDs of mostly approximately 20 nm (gray frequency of occurrence bars in Figure 10a). The blue dashed curve in Figure 10a represents an effective BC size distribution, normalized by CMDs, that is extracted from all grids, and the standard deviation is assumed to be 1.8. In contrast, different in-situ and laboratory observations show BC CMDs that are two to three times larger, that is, 50–80 nm, thus, a more reasonable CMD of 70 nm, as suggested by Bond et al. (2013), is considered in CAM6-ABC (blue solid curve in Figure 10a). Because BC normally has a small mass fraction among all aerosols (mostly under 10%), another byproduct of internally homogeneous mixing

19422466, 2023, 10, Downloaded from https://agupubs.onlinelibrary.wiley.com/doi/10.1029/2022MS003501 by Nanjing University Of, Wiley Online Library on [21/10/2023]. See the Terms and Conditions (https://onlinelibrary.wiley.com/terms-and-conditions) on Wiley Online Library for rules of use; OA articles are governed by the applicable Creative Commons License

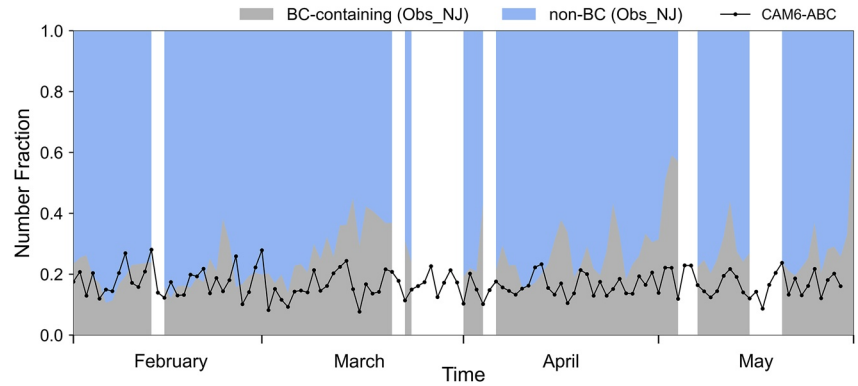

Figure 11. Daily average black carbon (BC)-containing particle number fractions from soot photometer observations and Community Atmosphere Model version 6 (CAM6)-Advanced Black Carbon (ABC) in Nanjing, China. The default CAM6 assumes that all particles in the accumulation mode contain the BC component, that is, a 100% BC-containing particle number fraction. Note that the unshaded regions represent missing observations.

is the overestimated BC CT, which also conflicts with the observations. Figure 10b shows the CT distributions that are simulated annually by CAM6-MAM4 and CAM6-ABC and the CT distributions from three cities, Nanjing, China (Obs_NJ), Tokyo, Japan (Obs_TK) and Sacramento, USA (Obs_SC), that are observed by SP2. The observations show median (black horizontal lines in Figure 10b) and geometric mean (red horizontal lines in Figure 10b) CTs of between 10 and 40 nm, while the default CAM6-MAM4 simulates a much thicker coating at ∼50 nm. This result implies that the CT derived through an internally homogeneous mixing model is overestimated. With larger BC sizes, the corresponding CT simulated by CAM6-ABC becomes thinner, decreasing to values that are closer to the observed ranges. Note that the dry CTs are used for comparison and do not involve hygroscopic calculations, which are derived from the BC and dry coating mass fraction.

Furthermore, Figure 11 shows a comparison of the daily average number fraction of BC-containing particles between the CAM-ABC and SP2 observations in Nanjing, China, in 2020. In this region, the BC-containing particle number fractions are generally less than 40%. The result indicates that the trend of the number fraction of BC-containing particles that is simulated by CAM-ABC is consistent with the measurement. The blank space indicates missing measurements. In CAM6, 100% of the accumulation mode particles are BC-containing because the modal-based scheme assumes that BC components are uniformly and homogeneously mixed. Note that our simulations are more representative of urban samples since BC emitted from biomass burning (BB) is typically larger in size than that from urban emissions (Schwarz et al., 2008). Dumka et al. (2018) summarizes the contribution of FF combustion and BB to BC concentration from previous studies in East Asia, India, Europe and North America. The results show that fossil fuels are dominant in over 80% of the sites with over 70% BC_{FF} contribution. Therefore, FF is dominant in most cities worldwide except BB-dominated regions, such as middle Africa. With the FF-emitted BC size distribution from the in-situ observations and its mass concentration provided by CAM6 simulations, we can estimate the BC number concentration directly instead of distributing the BC mass among all aerosol particles. The observed BC size distribution, in which the CMD is 70 nm with a standard deviation of 1.8 (Bond et al., 2013), is employed in CAM6-ABC for a more accurate CT.

4.2. BC Optical Properties

The BC absorption aerosol optical depth (AAOD) in CAM6-ABC and CAM6-MAM4, caused by BC mixing states and optical parameterizations, is shown in Figure 12. Since our modification is aimed at the BC mixing state and microphysical properties in the aerosol module, the BC AAOD at 550 nm from BC emission sources in middle Africa, eastern China, India and southern America are selected for comparison. As the online simulation shows, BC AAOD at 550 nm shows an apparent distinction in the two models, with regional mean values of 0.0114 (CAM6-MAM4) and 0.0081 (CAM6-ABC). The mean BC AAOD in homogeneous mixing by optical parameterization is 29% larger than that in new BC CS mixing (CAM6-ABC). The results indicate that the BC in the homogeneous mixing model absorbs more solar energy than that in the CS model.

The observation-constrained treatments for BC properties in the optical simulations are expected to alleviate the overestimation of BC absorption. The global E_{abs} distributions from the default CAM6-MAM4 and the

19422466, 2023, 10, Downloaded from https://agupubs.onlinelibrary.wiley.com/doi/10.1029/2022MS003501 by Nanjing University Of, Wiley Online Library on [21/10/2023]. See the Terms and Conditions (https://onlinelibrary.wiley.com/terms-and-conditions) on Wiley Online Library for rules of use; OA articles are governed by the applicable Creative Commons License

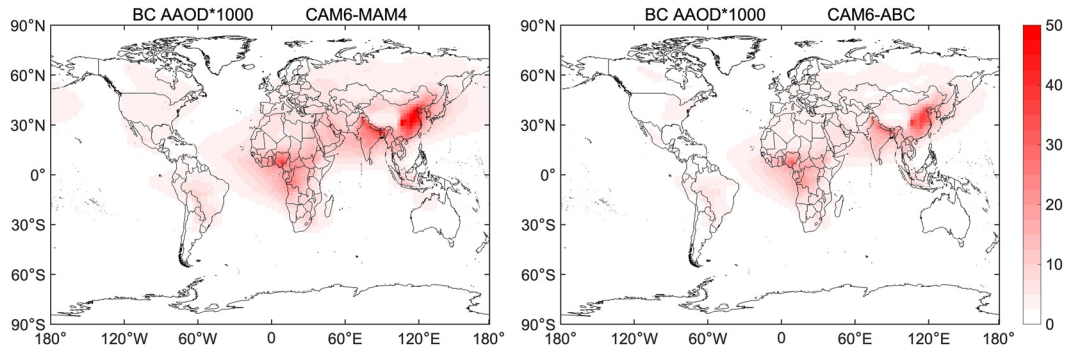

Figure 12. Global distribution of modeled black carbon (BC) absorption aerosol optical depth (AAOD) in Community Atmosphere Model version 6 (CAM6)-Modal Aerosol Model version 4 (MAM4) and CAM6-Advanced Black Carbon (ABC) at 550 nm.

CAM6-ABC model are illustrated in Figures 13a and 13b. The white region represents a BC mass fraction of less than 2% in the accumulation mode. We calculate the MAC at 550 nm of fresh uncoated BC offline, which varies with different CMDs in CAM6-MAM4 and is 5.9 m^2/g with a CMD of 70 nm in CAM6-ABC. The BC near the source regions exhibits smaller E_{abs} values because of its thinner CT. For the same reason, larger E_{abs} values over the ocean are attributed to further enhancement due to the hygroscopic growth of aerosol particles. Figure 13c shows the modeled E_{abs} values at 550 nm as a function of the BC mass fraction among the aerosol mass in the accumulation mode, as well as values reported in previous observations (see Table 1) (Cappa et al., 2012, 2019; Lack et al., 2012; Lan et al., 2013; D. Liu et al., 2017; Ma et al., 2020; Taylor et al., 2020; Ueda et al., 2016; C. Wu et al., 2018). The results indicate that the E_{abs} value in the online simulation decreases with increasing BC mass fraction in the accumulation mode (Figure 13c). The default CAM6-MAM4 simulations (blue dots) overestimate E_{abs}, with most of the values being larger than 2 and as large as 3, while the modeled E_{abs} by CAM6-ABC (red dots) varies between 1 and 2, with a global average of ~1.4. The new BC treatment (CAM6-ABC) performs better than CAM6-MAM4 since its E_{abs} values fall within the range of worldwide observations.

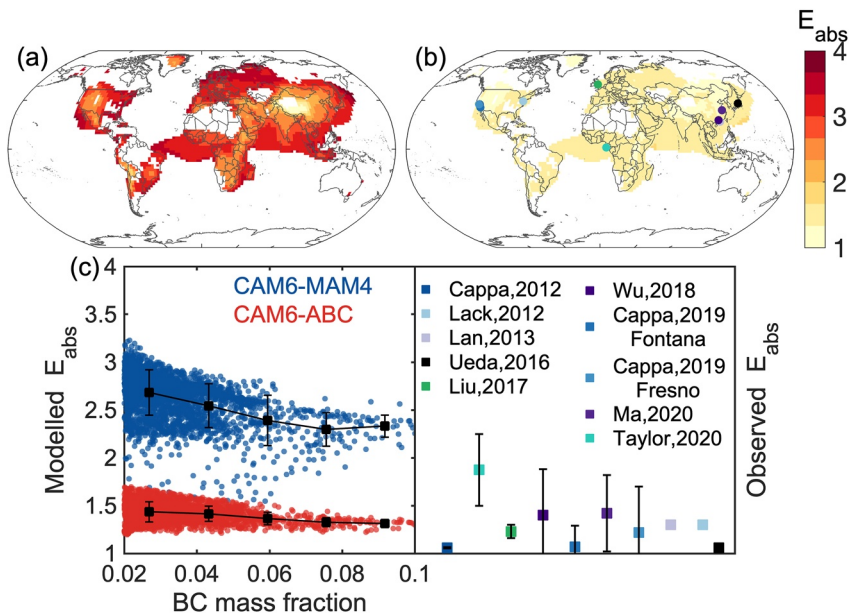

Figure 13. Comparison between modeled and observed absorption enhancement (E_{abs}). (a) E_{abs} distribution at the surface level from the default Community Atmosphere Model version 6 (CAM6)-Modal Aerosol Model version 4 (MAM4) model. (b) E_{abs} distribution at the surface level from the CAM6-Advanced Black Carbon (ABC) model. Only results with a black carbon (BC) mass fraction in the accumulation mode that is greater than 2% are presented in (a) and (b). (c) E_{abs} as a function of the mass fraction of BC out of total aerosols in the accumulation mode and the E_{abs} values from global in situ observations. The colored dots (b) indicate the observation locations.

19422466, 2023, 10, Downloaded from https://agupubs.onlinelibrary.wiley.com/doi/10.1029/2022MS003501 by Nanjing University Of, Wiley Online Library on [21/10/2023]. See the Terms and Conditions (https://onlinelibrary.wiley.com/terms-and-conditions) on Wiley Online Library for rules of use; OA articles are governed by the applicable Creative Commons License

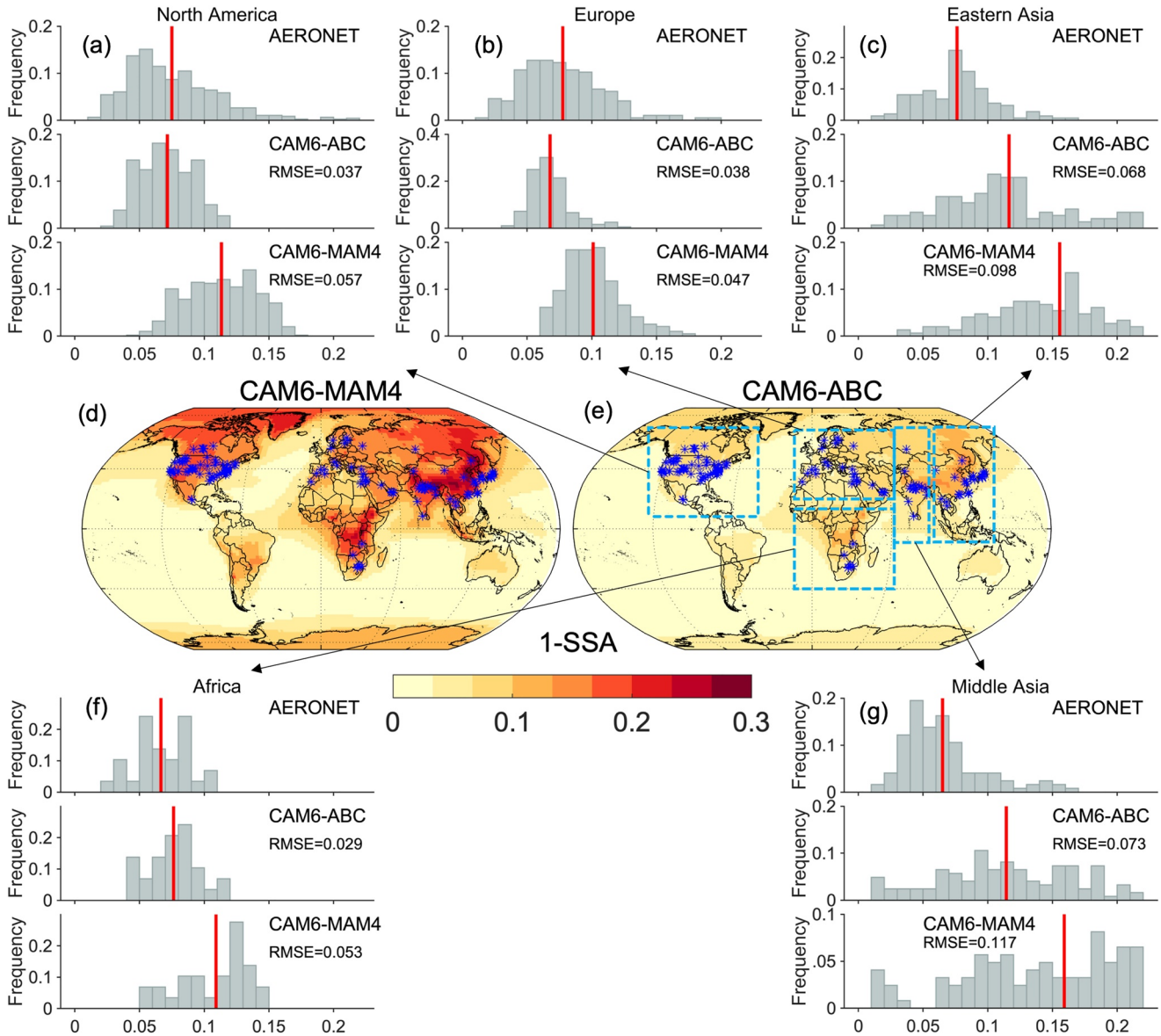

Figure 14. Comparison between modeled and measured single-scattering coalbedo (1 − single-scattering albedo [SSA]) at 550 nm. Comparison of the 1 − SSA distribution between the Aerosol Robotic Network (AERONET) observations and the Community Atmosphere Model version 6 (CAM6)-Modal Aerosol Model version 4 (MAM4) and CAM6-Advanced Black Carbon (ABC) model results over (a) North America, (b) Europe, (c) Eastern Asia, (f) Africa and (g) Middle Asia. (d, e) The 1 − SSA of the global spatial distribution simulated by the CAM6-MAM4 and CAM6-ABC models. Red lines represent mean values. These monthly mean values are from 169 stations from 2011 to 2016.

4.3. Overall Aerosol Absorption

As a major contributor to aerosol overall light absorption, BC may hold over 60% of the AAOD in the AeroCom phase III global models (Sand et al., 2021). Since the BC mass in the accumulation mode contributes over 80% of the total BC mass, our CAM6-ABC model also improves the overall aerosol light absorption simulations. Unlike BC aerosols, the overall aerosol scattering is much stronger than the absorption in the atmosphere, represented by SSA values of mainly 0.8 to 1. To present the absorption change that is induced by BC, we directly compare the modeled single-scattering coalbedo (1 − SSA, fraction of aerosol light absorption among its extinction) with the global AERONET observations. The 1 − SSA of the entire column in the atmosphere is simulated, and the 1 − SSA results match the corresponding global AERONET sites. Figures 14d and 14e compares the global 1 − SSA that is annually simulated by CAM6-MAM4 and CAM6-ABC at 550 nm. The largest 1 − SSA can reach 0.2, which is largely distributed in areas of high soot content in Asia, Middle Africa and North America. The

19422466, 2023, 10, Downloaded from https://agupubs.onlinelibrary.wiley.com/doi/10.1029/2022MS003501 by Nanjing University Of, Wiley Online Library on [21/10/2023]. See the Terms and Conditions (https://onlinelibrary.wiley.com/terms-and-conditions) on Wiley Online Library for rules of use; OA articles are governed by the applicable Creative Commons License

19422466, 2023, 10, Downloaded from https://agupubs.onlinelibrary.wiley.com/doi/10.1029/2022MS003501 by Nanjing University Of, Wiley Online Library on [21/10/2023]. See the Terms and Conditions (https://onlinelibrary.wiley.com/terms-and-conditions) on Wiley Online Library for rules of use; OA articles are governed by the applicable Creative Commons License

monthly mean values from 2011 to 2016 from 169 AERONET stations are collocated for comparison with the modeled monthly 1 − SSA over five regions, that is, North America, Europe, Eastern Asia, Africa and Middle Asia (Figure 14). The ABC module clearly predicts aerosol absorption more accurately, and 1 − SSA from the CAM6-ABC simulation shows better agreement with AERONET observations. The mean 1 − SSA over the 169 stations is reduced from 0.12 to 0.08, with an average value of 0.07, in AERONET. The biases of the modeled mean values are reduced by 47%, 18%, 51%, 49%, and 69% over the four regions above, respectively. The root mean square errors (RMSEs) decrease by 33%, from 0.0726 (CAM6-MAM4) to 0.0486 (CAM6-ABC). For high BC emission regions in east Asia and middle Asia, although the CAM6-ABC model has improved the simulation of overall aerosol absorption, there still exists a gap between the simulations and AERONET observations. This finding is mainly due to the overlarge BC refractive index, some BC emissions from BB and the lack of a brown carbon component in CAM6. Specifically, the BC refractive index in CAM6 is too absorbing to represent the complex BC aging process. The CAM6-ABC model has difficulty accurately simulating BC absorption in regions dominated by BB BC, especially in middle Asia. Although brown carbon absorbs strongly in ultraviolet wavelengths with less effect on SSA at 550 nm (Feng et al., 2013), the lens effect for the BC core may still be influenced by brown carbon.

Previous studies have improved the aerosol optical model for the BC mixing state and showed similar improvements to our results. For example, a particle-resolved aerosol model PartMC-MOSAIC is used to quantify the impact of the aerosol mixing state on aerosol optical properties (Riemer et al., 2009). Based on simulations of PartMC-MOSAIC, Yao et al. (2022) found that assuming the aerosol to be internally mixed within prescribed size bins caused underestimations of aerosol scattering, leading to errors in the SSA of up to −22.3%. Matsui (2017) developed a 2-D sectional global aerosol model with 8 BC mixing state bins and implemented it in CAM5. His results showed that the global mean AAOD is reduced by 15% by resolving the BC mixing state. In summary, these studies show a decreasing modeled aerosol absorption after constraining the BC mixing state, which is consistent with our results. Note that it is difficult to apply the particle-resolved aerosol model with a high computational burden to CAM6. Our developed aerosol optical representation in CAM6 focuses on the BC mixing state and inhomogeneous distributions, unlike a brand new aerosol framework, such as the one employed in Matsui (2017).

AAOD is not used to evaluate the ABC model because the modeled AAOD is mainly influenced by two components: BC mass concentration/loading and BC absorption efficiency (i.e., its MAC). Thus, a comparison of modeled and observed AAOD may be unfair considering the significant uncertainties in BC mass concentrations in the model. Moreover, previous studies showed that AAOD may be underestimated by atmospheric models due to underestimated BC and OC emissions (C. Chen et al., 2019; Matsui & Mahowald, 2017; Schutgens & Zhong, 2021; Y. Wang et al., 2018). Thus, to minimize the impact of biases in aerosol mass concentration, we focus on the absorption per BC mass (MAC as well as E_{abs}) and the absorption fraction (i.e., 1 − SSA), both of which are independent of BC concentrations.

4.4. Revising the BC Radiative Effects

After modifying the BC microphysical and mixing properties, the BC-induced radiative effects also show significant changes in the CAM6-ABC model. The direct radiative effect (DRE) is typically estimated to explore BC aerosol interactions, that is, the flux perturbation with the entire present-day BC mass. To reveal the aerosol-radiation interaction, we consider the clear-sky BC DRE, which is defined as the difference in the net radiative flux with all species and that with all species except BC. The BC DREs at the top and bottom of the atmosphere (TOA and BOA, respectively) and in the atmosphere (ATMOS) have different warming and cooling effects. The BC in the ATMOS is the difference between the BC at the TOA and BOA. Figure 15 shows the spatial distribution of the BC DRE at the TOA, BOA and ATMOS for the default CAM6-MAM4 and CAM6-ABC simulations, averaged over 3 years (2013–2015). Both models for BC DRE show the same global distribution, with dominant regions over Middle Africa, India and eastern China (Figures 15a–15f). The CAM-MAM4 model simulates a positive BC DRE both at the TOA (0.37 W/m^2) and in the ATMOS (1.10 W/m^2) but a negative BC DRE at the BOA (−0.73 W/m^2). By better representing the BC properties, the BC light absorption is reduced, and the magnitudes of its TOA, BOA and ATMOS DREs are all reduced accordingly. There are globally averaged DRE reductions of 0.09 W/m^2 (by 24%) at the TOA, −0.08 W/m^2 (by 11%) at the BOA, and 0.17 W/m^2 (by 15%) in the ATMOS; in the BC source regions, compared with CAM6-MAM4, the BC TOA DRE of CAM6-ABC is 20%, 19% and 21%

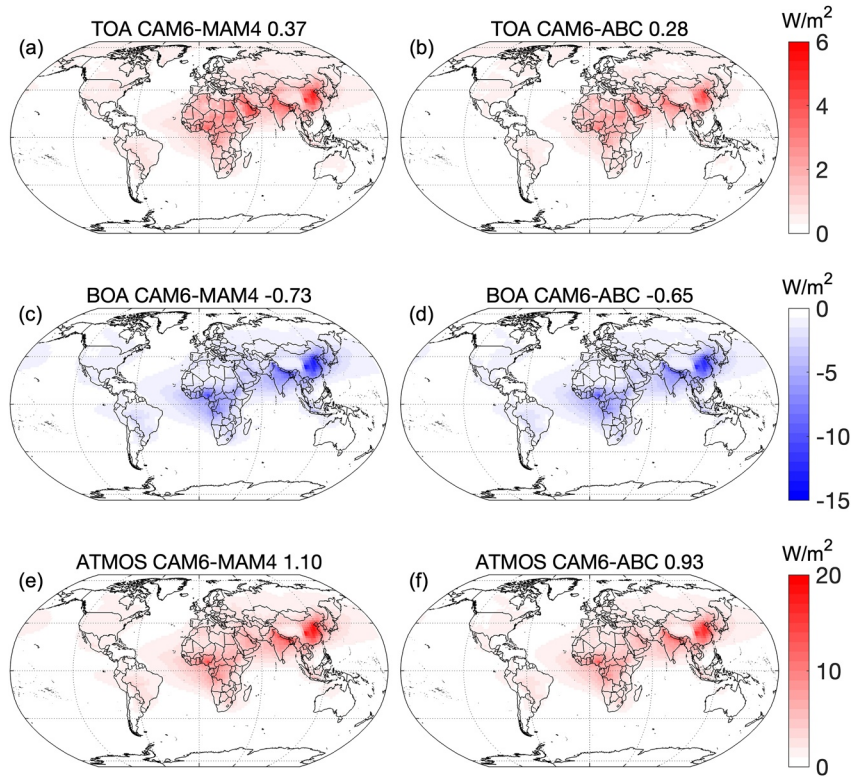

Figure 15. Modeled global black carbon (BC) clear-sky radiative effect from the default and new methods. (a, b) Default and Advanced Black Carbon (ABC)-modeled Community Atmosphere Model version 6 (CAM6) BC direct radiative effect (DRE) at the top of the atmosphere (TOA). (c, d) Default and ABC-modeled CAM6 BC DRE at the bottom of the atmosphere (BOA). (e, f) Default and ABC-modeled CAM6 BC DRE in the atmosphere (ATMOS). The globally averaged BC DRE at the TOA, BOA, and ATMOS changes from 0.37 to 0.28 W/m^2, −0.73 to −0.65 W/m^2, and 1.10 to 0.93 W/m^2, respectively.

smaller over Middle Africa, India and eastern China, respectively. This phenomenon can be explained by the fact that the weaker BC absorption in CAM6-ABC leads to more radiation scattering back to space, accounting for weaker net warming at the TOA (Figures 15a and 15b). More BC-induced radiation transmitted to the surface offsets some of the cooling effect at the BOA (Figures 15c and 15d).

To better understand the differences, we analyze the BC optical-radiative relationship in CAM6-MAM4 and CAM6-ABC. In BC emission regions, the BC AAOD from CAM6-ABC is mainly distributed in smaller ranges compared with CAM6-MAM4 (Figure 16b), whose distribution characteristics are the same as those of BC TOA DRE (Figure 16a). To quantify the optical-radiative differences, Figure 17 shows the BC AAOD and TOA DRE change from CAM6-MAM4 to CAM6-ABC. The linear correlation between ΔBC AAOD and ΔBC DRE is established. The results in Figure 17a indicate that the maximum variation in BC AAOD can reach 0.014, accounting for a maximum of 0.92 W/m^2 of BC TOA DRE. The ΔBC AAOD and ΔBC DRE in over 80% of the grids are less than 0.005 and 0.4 W/m^2, respectively. The larger BC AAOD change from CAM6-MAM4 to CAM6-ABC leads to a larger BC TOA DRE difference and has the following linear relationship: ΔBC DRE = 0.0622 × ΔBC AAOD + 0.0501. The two variables, ΔBC DRE and ΔBC AAOD, show a high linear correlation, for which the coefficient of determination (R^2) is 0.94. The BC optical impact on BC DRE in the ABC module can be represented by the fitting expression. Furthermore, the relative differences in BC AAOD and BC TOA DRE can both reach 50%, mainly ranging from 20% to 30% (Figure 17b).

5. Conclusions

We develop a new aerosol optical module entitled ABC for CAM6-MAM4, combining comprehensive observations and state-of-the-art numerical simulations for aerosol optical properties. In the ABC module, three major improvements in BC properties are achieved based on observational data. First, BC core sizes after emissions are larger than the current setting of CAM6. A lognormal distribution with a CMD of 70 nm and a standard deviation

19422466, 2023, 10, Downloaded from https://agupubs.onlinelibrary.wiley.com/doi/10.1029/2022MS003501 by Nanjing University Of, Wiley Online Library on [21/10/2023]. See the Terms and Conditions (https://onlinelibrary.wiley.com/terms-and-conditions) on Wiley Online Library for rules of use; OA articles are governed by the applicable Creative Commons License

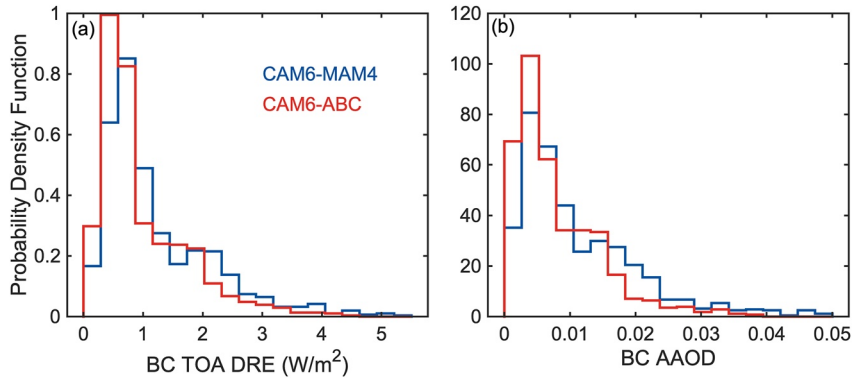

Figure 16. Distributions of black carbon (BC) top of the atmosphere (TOA) direct radiative effect (DRE) (a) and BC absorption aerosol optical depth (AAOD) (b) of Community Atmosphere Model version 6 (CAM6)-Modal Aerosol Model version 4 (MAM4) and CAM6-Advanced Black Carbon (ABC). The simulation results from BC emission sources at 550 nm are selected.

of 1.8 based on observations (Bond et al., 2013) is applied to the BC core size distribution in CAM6-ABC. Second, a representation of the heterogeneity of BC mixing states is developed. A fraction of non-BC aerosols is considered instead of the volume internal mixing assumption. For BC-containing particles, the mixing assumption that different-sized BC particles have similar CTs as their ages are applied to determine how the BC particles mix with other components. To verify the mixing assumption, BC size and CT observed by a single particle SP2 and the corresponding BC optical properties in online and offline simulations are analyzed. The observed BC CTs in Nanjing, Tokyo, and Sacramento are nearly invariable with BC core size (Figure 2) and show better agreement with CAM6-ABC than with CAM6-MAM4 (Figure 10). Thus, based on the above mixing assumption, the ABC module is not only consistent with microphysical observations but also avoids unnecessary computational costs caused by an excessively complex BC mixing representation. Third, an improved CS mixture optical algorithm with correction of BC morphology is established. We develop a CS model based on BC aggregates with predefined scaling factors of 0.97 and 1.03 for BC absorption and extinction, respectively.

Sensitivity simulations for different BC mixing states (internally homogeneous mixing and CS mixing) and different aerosol optical algorithms (parameterizations (Ghan & Zaveri, 2007) and Mie theory) are conducted to evaluate BC absorption. Compared with the homogeneous mixing by the default parameterizations in CAM6-MAM4, the mean BC AAOD at 550 nm in CAM6-ABC is reduced by 29%. Note that regions with high BC emissions over Africa, eastern China, India and southern America are selected for the comparison of BC AAOD.

We find that CAM6-MAM4, which uniformly distributes BC components among all aerosol particles, simulates a very small BC size and a thick coating for each particle and produces absorption enhancement (E_{abs}) values that

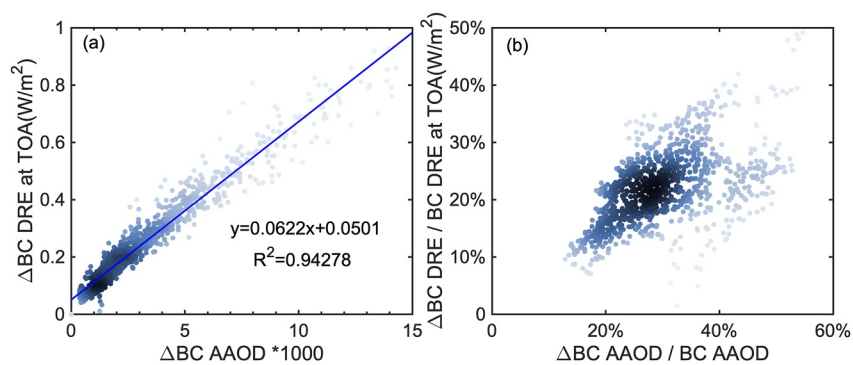

Figure 17. (a) Clear-sky black carbon (BC) top of the atmosphere (TOA) direct radiative effect (DRE) difference between Community Atmosphere Model version 6 (CAM6)-Modal Aerosol Model version 4 (MAM4) and CAM6-Advanced Black Carbon (ABC) as a function of the BC absorption aerosol optical depth (AAOD) difference between the two models. (b) Clear-sky relative difference in the BC DRE as a function of the relative difference in the BC AAOD. The blue line is a fitting line.

19422466, 2023, 10, Downloaded from https://agupubs.onlinelibrary.wiley.com/doi/10.1029/2022MS003501 by Nanjing University Of, Wiley Online Library on [21/10/2023]. See the Terms and Conditions (https://onlinelibrary.wiley.com/terms-and-conditions) on Wiley Online Library for rules of use; OA articles are governed by the applicable Creative Commons License

19422466, 2023, 10, Downloaded from https://agupubs.onlinelibrary.wiley.com/doi/10.1029/2022MS003501 by Nanjing University Of, Wiley Online Library on [21/10/2023]. See the Terms and Conditions (https://onlinelibrary.wiley.com/terms-and-conditions) on Wiley Online Library for rules of use; OA articles are governed by the applicable Creative Commons License

are significantly larger than the observational values. In contrast, ABC accounts for the observation-constrained BC size, mixing states and complex morphology in the CAM6 aerosol optical property simulations; thus, it improves the representation of aerosol light absorption and BC E_{abs} when compared with global observations. The E_{abs} values in CAM6-MAM4 are reduced from highly overestimated 2–3 to 1–2 by CAM6-ABC, which is closer to the global observations. Moreover, the simulation results of the single-scattering coalbedo using the MAM4 and ABC modules are compared with in situ (AERONET) data. The ABC module has a smaller mean single-scattering coalbedo than the MAM4 module, with better agreement with AERONET observations, reducing 47%, 18%, 51%, 49%, and 69% of the coalbedo biases over North America, Europe, Eastern Asia, Africa and Middle Asia, respectively. Compared with the AERONET observations, the RMSEs of the single-scattering coalbedo decrease by 33%, from 0.0726 (CAM6-MAM4) to 0.0486 (CAM6-ABC). The BC-induced warming effect weakens as BC absorption decreases. With less absorption due to BC and its mixing state, the semidirect effects are also weakened. The BC DRE is reduced by 11%–24% from CAM6-MAM4 to CAM6-ABC. More importantly, such modification is independent of aerosol chemical and microphysical procedures and can be implemented easily in models with different scales without a significantly increased computational burden.

The aerosol optical simulation in CAM6-ABC is improved by optimizing the aerosol representation of BC microphysical properties and mixing states, independent of the BC emission inventory. The BC emission inventory using CM3 Intercomparison Project Phase 6 emissions currently produces large uncertainties in the MAM4 simulation (Y. Wang et al., 2018). Thus, different BC emission sources and sizes can be considered in aerosol optical modules to improve the simulation of BC properties in future work.

Data Availability Statement

The CESM version 2.1.3 source codes in this study are publicly available online through Danabasoglu et al. (2020). The aerosol SSA data can be obtained from ground-based sun-photometer sites, AERONET (Dubovik & King, 2000; Holben et al., 1998). The modified climate model source codes for this study are available on Zenodo at https://doi.org/10.5281/zenodo.7947080 (G. Chen et al., 2023). Our analytic data that provide the major results are available at figshare at https://doi.org/10.6084/m9.figshare.21482961.v1 (G. Chen et al., 2022).

Acknowledgments
This work was supported through the National Key R&D Program of China (2022YFC3701000, Task 5), the Natural Science Foundation of China (Grants 42075098 and 42005082), and the Postgraduate Research and Practice Innovation Program of Jiangsu Province (KYCX21_0971). We thank the US Department of Energy (DOE) Atmospheric Radiation Measurement (ARM) program's Carbonaceous Aerosol and Radiative Effects Study (CARES) for their SP2 observations over SC, USA, and Dr. Nobuhiro Moteki for the SP2 observations over TK, Japan. We acknowledge the High Performance Computing Center of Nanjing University of Information Science and Technology for their support of this work.

References

Adachi, K., Chung, S. H., & Buseck, P. R. (2010). Shapes of soot aerosol particles and implications for their effects on climate. *Journal of Geophysical Research*, *115*(D15), D15206. https://doi.org/10.1029/2009JD012868

Aquila, V., Hendricks, J., Lauer, A., Riemer, N., Vogel, H., Baumgardner, D., et al. (2011). MADE-in: A new aerosol microphysics submodel for global simulation of insoluble particles and their mixing state. *Geoscientific Model Development*, *4*(2), 325–355. https://doi.org/10.5194/gmd-4-325-2011

Bauer, S. E., Menon, S., Koch, D., Bond, T. C., & Tsigaridis, K. (2010). A global modeling study on carbonaceous aerosol microphysical characteristics and radiative effects. *Atmospheric Chemistry and Physics*, *10*(15), 7439–7456. https://doi.org/10.5194/acp-10-7439-2010

Bauer, S. E., Wright, D. L., Koch, D., Lewis, E. R., McGraw, R., Chang, L. S., et al. (2008). MATRIX (Multiconfiguration Aerosol TRacker of mIXing state): An aerosol microphysical module for global atmospheric models. *Atmospheric Chemistry and Physics*, *8*(20), 6003–6035. https://doi.org/10.5194/acp-8-6003-2008

Bond, T. C., Doherty, S. J., Fahey, D. W., Forster, P. M., Berntsen, T., DeAngelo, B. J., et al. (2013). Bounding the role of black carbon in the climate system: A scientific assessment. *Journal of Geophysical Research: Atmospheres*, *118*(11), 5380–5552. https://doi.org/10.1002/jgrd.50171

Brown, H., Liu, X., Pokhrel, R., Murphy, S., Lu, Z., Saleh, R., et al. (2021). Biomass burning aerosols in most climate models are too absorbing. *Nature Communications*, *12*(1), 277. https://doi.org/10.1038/s41467-020-20482-9

Cappa, C. D., Onasch, T. B., Massoli, P., Worsnop, D. R., Bates, T. S., Cross, E. S., et al. (2012). Radiative absorption enhancements due to the mixing state of atmospheric black carbon. *Science*, *337*(6098), 1078–1081. https://doi.org/10.1126/science.1223447

Cappa, C. D., Onasch, T. B., Massoli, P., Worsnop, D. R., Bates, T. S., Cross, E. S., et al. (2013). Response to comment on "Radiative absorption enhancements due to the mixing state of atmospheric black carbon". *Science*, *339*(6118), 393. https://doi.org/10.1126/science.1230260

Cappa, C. D., Zhang, X., Russell, L. M., Collier, S., Lee, A. K. Y., Chen, C.-L., et al. (2019). Light absorption by ambient black and brown carbon and its dependence on black carbon coating state for two California, USA, cities in winter and summer. *Journal of Geophysical Research: Atmospheres*, *124*(3), 1550–1577. https://doi.org/10.1029/2018jd029501

Chakrabarty, R. K., Beres, N. D., Moosmuller, H., China, S., Mazzoleni, C., Dubey, M. K., et al. (2014). Soot superaggregates from flaming wildfires and their direct radiative forcing. *Scientific Reports*, *4*(1), 5508. https://doi.org/10.1038/srep05508

Chakrabarty, R. K., & Heinson, W. R. (2018). Scaling laws for light absorption enhancement due to nonrefractory coating of atmospheric black carbon aerosol. *Physical Review Letters*, *121*(21), 218701. https://doi.org/10.1103/PhysRevLett.121.218701

Chakrabarty, R. K., Moosmüller, H., Arnott, W. P., Garro, M. A., Slowik, J. G., Cross, E. S., et al. (2007). Light scattering and absorption by fractal-like carbonaceous chain aggregates: Comparison of theories and experiment. *Applied Optics*, *46*(28), 6990–7006. https://doi.org/10.1364/AO.46.006990

Chen, C., Dubovik, O., Henze, D. K., Chin, M., Lapyonok, T., Schuster, G. L., et al. (2019). Constraining global aerosol emissions using POLDER/PARASOL satellite remote sensing observations. *Atmospheric Chemistry and Physics*, *19*(23), 14585–14606. https://doi.org/10.5194/acp-19-14585-2019

Chen, G., Wang, J., Wang, Y., Wang, J., Jin, Y., Cheng, Y., et al. (2022). Analytic data of figures [Dataset]. Figshare. https://doi.org/10.6084/m9.figshare.21482961.v1

Chen, G., Wang, J., Wang, Y., Wang, J., Jin, Y., Cheng, Y., et al. (2023). Advanced black carbon module in Community Atmosphere Model version 6 (CAM6-ABC) source codes and data [Dataset]. Zenodo. https://doi.org/10.5281/zenodo.7947080

Chen, L., Zhang, F., Yan, P., Wang, X., Sun, L., Li, Y., et al. (2020). The large proportion of black carbon (BC)-containing aerosols in the urban atmosphere. *Environmental Pollution*, *263*(Pt B), 114507. https://doi.org/10.1016/j.envpol.2020.114507

China, S., Mazzoleni, C., Gorkowski, K., Aiken, A. C., & Dubey, M. K. (2013). Morphology and mixing state of individual freshly emitted wildfire carbonaceous particles. *Nature Communications*, *4*(1), 2122. https://doi.org/10.1038/ncomms3122

Curtis, J. H., Riemer, N., & West, M. (2017). A single-column particle-resolved model for simulating the vertical distribution of aerosol mixing state: WRF-PartMC-MOSAIC-SCM v1.0. *Geoscientific Model Development*, *10*(11), 4057–4079. https://doi.org/10.5194/gmd-10-4057-2017

Danabasoglu, G., Lamarque, J. F., Bacmeister, J., Bailey, D. A., DuVivier, A. K., Edwards, J., et al. (2020). The Community Earth System Model Version 2 (CESM2). *Journal of Advances in Modeling Earth Systems*, *12*(2), e2019MS001916. https://doi.org/10.1029/2019ms001916

Dubovik, O., & King, M. D. (2000). A flexible inversion algorithm for retrieval of aerosol optical properties from Sun and sky radiance measurements. *Journal of Geophysical Research*, *105*(D16), 20673–20696. https://doi.org/10.1029/2000jd900282

Dumka, U., Kaskaoutis, D., Tiwari, S., Safai, P., Attri, S., Soni, V., et al. (2018). Assessment of biomass burning and fossil fuel contribution to black carbon concentrations in Delhi during winter. *Atmospheric Environment*, *194*, 93–109. https://doi.org/10.1016/j.atmosenv.2018.09.033

Feng, Y., Ramanathan, V., & Kotamarthi, V. R. (2013). Brown carbon: A significant atmospheric absorber of solar radiation? *Atmospheric Chemistry and Physics*, *13*(17), 8607–8621. https://doi.org/10.5194/acp-13-8607-2013

Fierce, L., Bond, T. C., Bauer, S. E., Mena, F., & Riemer, N. (2016). Black carbon absorption at the global scale is affected by particle-scale diversity in composition. *Nature Communications*, *7*(1), 12361. https://doi.org/10.1038/ncomms12361

Gao, R. S., Schwarz, J. P., Kelly, K. K., Fahey, D. W., Watts, L. A., Thompson, T. L., et al. (2007). A Novel method for estimating light-scattering properties of soot aerosols using a modified single-particle soot photometer. *Aerosol Science and Technology*, *41*(2), 125–135. https://doi.org/10.1080/02786820601118398

Ghan, S. J., & Zaveri, R. A. (2007). Parameterization of optical properties for hydrated internally mixed aerosol. *Journal of Geophysical Research*, *112*(D10), D10201. https://doi.org/10.1029/2006jd007927

Gong, S. L., Barrie, L., Blanchet, J. P., Von Salzen, K., Lohmann, U., Lesins, G., et al. (2003). Canadian Aerosol Module: A size-segregated simulation of atmospheric aerosol processes for climate and air quality models 1. Module development. *Journal of Geophysical Research*, *108*(D1), 4007. https://doi.org/10.1029/2001JD002002

Gong, S. L., Barrie, L. A., & Lazare, M. (2002). Canadian Aerosol Module (CAM): A size-segregated simulation of atmospheric aerosol processes for climate and air quality models 2. Global sea-salt aerosol and its budgets. *Journal of Geophysical Research*, *107*(D24), 4779. https://doi.org/10.1029/2001jd002004

Holben, B. N., Eck, T. F., Slutsker, I., Tanré, D., Buis, J. P., Setzer, A., et al. (1998). AERONET—A federated instrument network and data archive for aerosol characterization. *Remote Sensing of Environment*, *66*(1), 1–16. https://doi.org/10.1016/S0034-4257(98)00031-5

Jacobson, M. Z. (2001). Strong radiative heating due to the mixing state of black carbon in atmospheric aerosols. *Nature*, *409*(6821), 695–697. https://doi.org/10.1038/35055518

Knox, A., Evans, G. J., Brook, J. R., Yao, X., Jeong, C. H., Godri, K. J., et al. (2009). Mass absorption cross-section of ambient black carbon aerosol in relation to chemical age. *Aerosol Science and Technology*, *43*(6), 522–532. https://doi.org/10.1080/02786820902777207

Kokkola, H., Kühn, T., Laakso, A., Bergman, T., Lehtinen, K. E. J., Mielonen, T., et al. (2018). SALSA2.0: The sectional aerosol module of the aerosol–chemistry–climate model ECHAM6.3.0-HAM2.3-MOZ1.0. *Geoscientific Model Development*, *11*(9), 3833–3863. https://doi.org/10.5194/gmd-11-3833-2018

Kompalli, S. K., Suresh Babu, S. N., Satheesh, S. K., Krishna Moorthy, K., Das, T., Boopathy, R., et al. (2020). Seasonal contrast in size distributions and mixing state of black carbon and its association with $PM_{1.0}$ chemical composition from the eastern coast of India. *Atmospheric Chemistry and Physics*, *20*(6), 3965–3985. https://doi.org/10.5194/acp-20-3965-2020

Köylü, Ü. Ö., Faeth, G. M., Farias, T. L., & Carvalho, M. D. G. (1995). Fractal and projected structure properties of soot aggregates. *Combustion and Flame*, *100*(4), 621–633. https://doi.org/10.1016/0010-2180(94)00147-K

Krol, M., Houweling, S., Bregman, B., Van den Broek, M., Segers, A., Van Velthoven, P., et al. (2005). The two-way nested global chemistry-transport zoom model TM5: Algorithm and applications. *Atmospheric Chemistry and Physics*, *5*(2), 417–432. https://doi.org/10.5194/acp-5-417-2005

Lack, D. A., Langridge, J. M., Bahreini, R., Cappa, C. D., Middlebrook, A. M., & Schwarz, J. P. (2012). Brown carbon and internal mixing in biomass burning particles. *Proceedings of the National Academy of Sciences of the United States of America*, *109*(37), 14802–14807. https://doi.org/10.1073/pnas.1206575109

Lan, Z.-J., Huang, X.-F., Yu, K.-Y., Sun, T.-L., Zeng, L.-W., & Hu, M. (2013). Light absorption of black carbon aerosol and its enhancement by mixing state in an urban atmosphere in South China. *Atmospheric Environment*, *69*, 118–123. https://doi.org/10.1016/j.atmosenv.2012.12.009

Li, J., Pósfai, M., Hobbs, P. V., & Buseck, P. R. (2003). Individual aerosol particles from biomass burning in southern Africa: 2, Compositions and aging of inorganic particles. *Journal of Geophysical Research*, *108*(D13), 8484. https://doi.org/10.1029/2002jd002310

Li, T., Sattar, T. P., & Sun, S. (2012). Deterministic resampling: Unbiased sampling to avoid sample impoverishment in particle filters. *Signal Processing*, *92*(7), 1637–1645. https://doi.org/10.1016/j.sigpro.2011.12.019

Liu, C., Lee Panetta, R., & Yang, P. (2012). Application of the pseudo-spectral time domain method to compute particle single-scattering properties for size parameters up to 200. *Journal of Quantitative Spectroscopy and Radiative Transfer*, *113*(13), 1728–1740. https://doi.org/10.1016/j.jqsrt.2012.04.021

Liu, C., Li, J., Yin, Y., Zhu, B., & Feng, Q. (2017). Optical properties of black carbon aggregates with non-absorptive coating. *Journal of Quantitative Spectroscopy and Radiative Transfer*, *187*, 443–452. https://doi.org/10.1016/j.jqsrt.2016.10.023

Liu, C., Xu, X., Yin, Y., Schnaiter, M., & Yung, Y. L. (2019). Black carbon aggregates: A database for optical properties. *Journal of Quantitative Spectroscopy and Radiative Transfer*, *222*, 170–179. https://doi.org/10.1016/j.jqsrt.2018.10.021

Liu, D., Allan, J. D., Young, D. E., Coe, H., Beddows, D., Fleming, Z. L., et al. (2014). Size distribution, mixing state and source apportionment of black carbon aerosol in London during wintertime. *Atmospheric Chemistry and Physics*, *14*(18), 10061–10084. https://doi.org/10.5194/acp-14-10061-2014

Liu, D., Whitehead, J., Alfarra, M. R., Reyes-Villegas, E., Spracklen, D. V., Reddington, C. L., et al. (2017). Black-carbon absorption enhancement in the atmosphere determined by particle mixing state. *Nature Geoscience*, *10*(3), 184–188. https://doi.org/10.1038/ngeo2901

Liu, S., Aiken, A. C., Gorkowski, K., Dubey, M. K., Cappa, C. D., Williams, L. R., et al. (2015). Enhanced light absorption by mixed source black and brown carbon particles in UK winter. *Nature Communications*, *6*(1), 8435. https://doi.org/10.1038/ncomms9435

19422466, 2023, 10, Downloaded from https://agupubs.onlinelibrary.wiley.com/doi/10.1029/2022MS003501 by Nanjing University Of, Wiley Online Library on [21/10/2023]. See the Terms and Conditions (https://onlinelibrary.wiley.com/terms-and-conditions) on Wiley Online Library for rules of use; OA articles are governed by the applicable Creative Commons License

Liu, X., Easter, R. C., Ghan, S. J., Zaveri, R., Rasch, P., Shi, X., et al. (2012). Toward a minimal representation of aerosols in climate models: Description and evaluation in the Community Atmosphere Model CAM5. *Geoscientific Model Development*, *5*(3), 709–739. https://doi.org/10.5194/gmd-5-709-2012

Liu, X., Ma, P. L., Wang, H., Tilmes, S., Singh, B., Easter, R. C., et al. (2016). Description and evaluation of a new four-mode version of the Modal Aerosol Module (MAM4) within version 5.3 of the Community Atmosphere Model. *Geoscientific Model Development*, *9*(2), 505–522. https://doi.org/10.5194/gmd-9-505-2016

Luo, J., Zhang, Q., Luo, J., Liu, J., Huo, Y., & Zhang, Y. (2019). Optical modeling of black carbon with different coating materials: The effect of coating configurations. *Journal of Geophysical Research: Atmospheres*, *124*(23), 13230–13253. https://doi.org/10.1029/2019jd031701

Ma, Y., Huang, C., Jabbour, H., Zheng, Z., Wang, Y., Jiang, Y., et al. (2020). Mixing state and light absorption enhancement of black carbon aerosols in summertime Nanjing, China. *Atmospheric Environment*, *222*, 117141. https://doi.org/10.1016/j.atmosenv.2019.117141

Masson-Delmotte, V., Zhai, P., Pirani, A., Connors, S. L., Péan, C., Berger, S., et al. (2021). *IPCC, 2021: Climate change 2021: The physical science basis. Contribution of Working Group I to the sixth assessment report of the Intergovernmental Panel on Climate Change*. Cambridge University Press.

Matsui, H. (2017). Development of a global aerosol model using a two-dimensional sectional method: 1. Model design. *Journal of Advances in Modeling Earth Systems*, *9*(4), 1921–1947. https://doi.org/10.1002/2017MS000937

Matsui, H., Hamilton, D. S., & Mahowald, N. M. (2018). Black carbon radiative effects highly sensitive to emitted particle size when resolving mixing-state diversity. *Nature Communications*, *9*(1), 3446. https://doi.org/10.1038/s41467-018-05635-1

Matsui, H., Koike, M., Kondo, Y., Moteki, N., Fast, J. D., & Zaveri, R. A. (2013). Development and validation of a black carbon mixing state resolved three-dimensional model: Aging processes and radiative impact. *Journal of Geophysical Research: Atmospheres*, *118*(5), 2304–2326. https://doi.org/10.1029/2012jd018446

Matsui, H., & Mahowald, N. (2017). Development of a global aerosol model using a two-dimensional sectional method: 2. Evaluation and sensitivity simulations. *Journal of Advances in Modeling Earth Systems*, *9*(4), 1887–1920. https://doi.org/10.1002/2017ms000937

Mlawer, E. J., Taubman, S. J., Brown, P. D., Iacono, M. J., & Clough, S. A. (1997). Radiative transfer for inhomogeneous atmospheres: RRTM, a validated correlated-k model for the longwave. *Journal of Geophysical Research*, *102*(D14), 16663–16682. https://doi.org/10.1029/97JD00237

Moteki, N., Kondo, Y., & Adachi, K. (2014). Identification by single-particle soot photometer of black carbon particles attached to other particles: Laboratory experiments and ground observations in Tokyo. *Journal of Geophysical Research: Atmospheres*, *119*(2), 1031–1043. https://doi.org/10.1002/2013jd020655

Pachauri, R. K., Allen, M. R., Barros, V. R., Broome, J., Cramer, W., Christ, R., et al. (2014). *Climate change 2014: Synthesis report. Contribution of Working Groups I, II and III to the fifth assessment report of the Intergovernmental Panel on Climate Change*. Cambridge University Press.

Peng, J., Hu, M., Guo, S., Du, Z., Zheng, J., Shang, D., et al. (2016). Markedly enhanced absorption and direct radiative forcing of black carbon under polluted urban environments. *Proceedings of the National Academy of Sciences of the United States of America*, *113*(16), 4266–4271. https://doi.org/10.1073/pnas.1602310113

Ramanathan, V., Crutzen, P. J., Kiehl, J. T., & Rosenfeld, D. (2001). Aerosols, climate, and the hydrological cycle. *Science*, *294*(5549), 2119–2124. https://doi.org/10.1126/science.1064034

Riemer, N., Ault, A., West, M., Craig, R., & Curtis, J. (2019). Aerosol mixing state: Measurements, modeling, and impacts. *Reviews of Geophysics*, *57*(2), 187–249. https://doi.org/10.1029/2018RG000615

Riemer, N., West, M., Zaveri, R. A., & Easter, R. C. (2009). Simulating the evolution of soot mixing state with a particle-resolved aerosol model. *Journal of Geophysical Research*, *114*(D9), D09202. https://doi.org/10.1029/2008jd011073

Romshoo, B., Pöhlker, M., Wiedensohler, A., Pfeifer, S., Saturno, J., Nowak, A., et al. (2022). Importance of size representation and morphology in modelling optical properties of black carbon: Comparison between laboratory measurements and model simulations. *Atmospheric Measurement Techniques*, *15*(23), 6965–6989. https://doi.org/10.5194/amt-15-6965-2022

Sand, M., Samset, B. H., Myhre, G., Gliß, J., Bauer, S. E., Bian, H., et al. (2021). Aerosol absorption in global models from AeroCom phase III. *Atmospheric Chemistry and Physics*, *21*(20), 15929–15947. https://doi.org/10.5194/acp-21-15929-2021

Schnaiter, M., Linke, C., Möhler, O., Naumann, K. H., Saathoff, H., Wagner, R., et al. (2005). Absorption amplification of black carbon internally mixed with secondary organic aerosol. *Journal of Geophysical Research*, *110*(D19), D19204. https://doi.org/10.1029/2005JD006046

Schutgens, N., & Zhong, Q. (2021). AEROCOM/AEROSAT: An intercomparison of AAOD & SSA in model and satellite data. In *EGU General Assembly 2021*. EGU21-11992. https://doi.org/10.5194/egusphere-egu21-11992

Schwarz, J. P., Gao, R. S., Spackman, J. R., Watts, L. A., Thomson, D. S., Fahey, D. W., et al. (2008). Measurement of the mixing state, mass, and optical size of individual black carbon particles in urban and biomass burning emissions. *Geophysical Research Letters*, *35*(13), L13810. https://doi.org/10.1029/2008gl033968

Sedlacek, A. J., Onasch, T. B., Nichman, L., Lewis, E. R., Davidovits, P., Freedman, A., & Williams, L. (2018). Formation of refractory black carbon by SP2-induced charring of organic aerosol. *Aerosol Science and Technology*, *52*(12), 1345–1350. https://doi.org/10.1080/02786826.2018.1531107

Shetty, N., Beeler, P., Paik, T., Brechtel, F. J., & Chakrabarty, R. K. (2021). Bias in quantification of light absorption enhancement of black carbon aerosol coated with low-volatility brown carbon. *Aerosol Science and Technology*, *55*(5), 539–551. https://doi.org/10.1080/02786826.2021.1873909

Stier, P., Feichter, J., Kinne, S., Kloster, S., Vignati, E., Wilson, J., et al. (2005). The aerosol-climate model ECHAM5-HAM. *Atmospheric Chemistry and Physics*, *5*(4), 1125–1156. https://doi.org/10.5194/acp-5-1125-2005

Sun, J., Sun, Y., Xie, C., Xu, W., Chen, C., Wang, Z., et al. (2022). The chemical composition and mixing state of BC-containing particles and the implications on light absorption enhancement. *Atmospheric Chemistry and Physics*, *22*(11), 7619–7630. https://doi.org/10.5194/acp-22-7619-2022

Taylor, J. W., Wu, H., Szpek, K., Bower, K., Crawford, I., Flynn, M. J., et al. (2020). Absorption closure in highly aged biomass burning smoke. *Atmospheric Chemistry and Physics*, *20*(19), 11201–11221. https://doi.org/10.5194/acp-20-11201-2020

Thamban, N. M., Tripathi, S. N., Moosakutty, S. P., Kuntamukkala, P., & Kanawade, V. P. (2017). Internally mixed black carbon in the Indo-Gangetic Plain and its effect on absorption enhancement. *Atmospheric Research*, *197*, 211–223. https://doi.org/10.1016/j.atmosres.2017.07.007

Ueda, S., Nakayama, T., Taketani, F., Adachi, K., Matsuki, A., Iwamoto, Y., et al. (2016). Light absorption and morphological properties of soot-containing aerosols observed at an East Asian outflow site, Noto Peninsula, Japan. *Atmospheric Chemistry and Physics*, *16*(4), 2525–2541. https://doi.org/10.5194/acp-16-2525-2016

Wang, J., Wang, J., Cai, R., Liu, C., Jiang, J., Nie, W., et al. (2023). Unified theoretical framework for black carbon mixing state allows greater accuracy of climate effect estimation. *Nature Communications*, *14*(1), 2703. https://doi.org/10.1038/s41467-023-38330-x

19422466, 2023, 10, Downloaded from https://agupubs.onlinelibrary.wiley.com/doi/10.1029/2022MS003501 by Nanjing University Of, Wiley Online Library on [21/10/2023]. See the Terms and Conditions (https://onlinelibrary.wiley.com/terms-and-conditions) on Wiley Online Library for rules of use; OA articles are governed by the applicable Creative Commons License

Wang, X., Heald, C. L., Ridley, D. A., Schwarz, J. P., Spackman, J. R., Perring, A. E., et al. (2014). Exploiting simultaneous observational constraints on mass and absorption to estimate the global direct radiative forcing of black carbon and brown carbon. *Atmospheric Chemistry and Physics*, *14*(20), 10989–11010. https://doi.org/10.5194/acp-14-10989-2014

Wang, Y., Khalizov, A., Levy, M., & Zhang, R. (2013). New directions: Light absorbing aerosols and their atmospheric impacts. *Atmospheric Environment*, *81*, 713–715. https://doi.org/10.1016/j.atmosenv.2013.09.034

Wang, Y., Li, W., Huang, J., Liu, L., Pang, Y., He, C., et al. (2021). Nonlinear enhancement of radiative absorption by black carbon in response to particle mixing structure. *Geophysical Research Letters*, *48*(24), e2021GL096437. https://doi.org/10.1029/2021gl096437

Wang, Y., Liu, F., He, C., Bi, L., Cheng, T., Wang, Z., et al. (2017). Fractal dimensions and mixing structures of soot particles during atmospheric processing. *Environmental Science and Technology Letters*, *4*(11), 487–493. https://doi.org/10.1021/acs.estlett.7b00418

Wang, Y., Ma, P. L., Peng, J., Zhang, R., Jiang, J. H., Easter, R. C., & Yung, Y. L. (2018). Constraining aging processes of black carbon in the community atmosphere model using environmental chamber measurements. *Journal of Advances in Modeling Earth Systems*, *10*(10), 2514–2526. https://doi.org/10.1029/2018MS001387

Wu, C., Wu, D., & Yu, J. Z. (2018). Quantifying black carbon light absorption enhancement with a novel statistical approach. *Atmospheric Chemistry and Physics*, *18*(1), 289–309. https://doi.org/10.5194/acp-18-289-2018

Wu, Y., Cheng, T., Zheng, L., & Chen, H. (2016). Black carbon radiative forcing at TOA decreased during aging. *Scientific Reports*, *6*(1), 38592. https://doi.org/10.1038/srep38592

Yao, Y., Curtis, J. H., Ching, J., Zheng, Z., & Riemer, N. (2022). Quantifying the effects of mixing state on aerosol optical properties. *Atmospheric Chemistry and Physics*, *22*(14), 9265–9282. https://doi.org/10.5194/acp-22-9265-2022

Yurkin, M. A., & Hoekstra, A. G. (2011). The discrete-dipole-approximation code ADDA: Capabilities and known limitations. *Journal of Quantitative Spectroscopy and Radiative Transfer*, *112*(13), 2234–2247. https://doi.org/10.1016/j.jqsrt.2011.01.031

Yurkin, M. A., Maltsev, V. P., & Hoekstra, A. G. (2007). The discrete dipole approximation for simulation of light scattering by particles much larger than the wavelength. *Journal of Quantitative Spectroscopy and Radiative Transfer*, *106*(1–3), 546–557. https://doi.org/10.1016/j.jqsrt.2007.01.033

Zaveri, R. A., Barnard, J. C., Easter, R. C., Riemer, N., & West, M. (2010). Particle-resolved simulation of aerosol size, composition, mixing state, and the associated optical and cloud condensation nuclei activation properties in an evolving urban plume. *Journal of Geophysical Research*, *115*(D17), D17210. https://doi.org/10.1029/2009jd013616

Zaveri, R. A., Shaw, W. J., Cziczo, D. J., Schmid, B., Ferrare, R. A., Alexander, M. L., et al. (2012). Overview of the 2010 Carbonaceous Aerosols and Radiative Effects Study (CARES). *Atmospheric Chemistry and Physics*, *12*(16), 7647–7687. https://doi.org/10.5194/acp-12-7647-2012

Zeng, C., Liu, C., Li, J., Zhu, B., Yin, Y., & Wang, Y. (2019). Optical properties and radiative forcing of aged BC due to hygroscopic growth: Effects of the aggregate structure. *Journal of Geophysical Research: Atmospheres*, *124*(8), 4620–4633. https://doi.org/10.1029/2018jd029809

Zeng, F., Wittenberg, A. T., Winton, M., Wilson, R. J., Stouffer, R. J., Stern, W. F., et al. (2011). The dynamical core, physical parameterizations, and basic simulation characteristics of the atmospheric component AM3 of the GFDL Global Coupled Model CM3. *Journal of Climate*, *24*(13), 3484–3519. https://doi.org/10.1175/2011jcli3955.1

Zhang, Y., Su, H., Kecorius, S., Ma, N., Wang, Z., Sun, Y., et al. (2023). Extremely low-volatility organic coating leads to underestimation of black carbon climate impact. *One Earth*, *6*(2), 158–166. https://doi.org/10.1016/j.oneear.2023.01.009

19422466, 2023, 10, Downloaded from https://agupubs.onlinelibrary.wiley.com/doi/10.1029/2022MS003501 by Nanjing University Of, Wiley Online Library on [21/10/2023]. See the Terms and Conditions (https://onlinelibrary.wiley.com/terms-and-conditions) on Wiley Online Library for rules of use; OA articles are governed by the applicable Creative Commons License